Department of Finance
Faculty of Business and Economics

Working Paper Series

Default Risk Linkages in a Structural Credit Model

Jan Ericsson, Kristoffer Glover, Alexandre Jeanneret, Lucie Y. Lu

Working Paper No. 01/23
November 2023

Default Risk Linkages in a Structural Credit Model*

Jan Ericsson
McGill University

Kristoffer Glover
University of Technology Sydney

Alexandre Jeanneret
UNSW Business School

Lucie Y. Lu
University of Melbourne

November 14, 2023

*We are very grateful for comments and suggestions from Daniel Andrei, Antje Berndt, Ruchith Dissanayake (discussant), Michael Hasler, Evan Jo, Ella Patelli, Maxime Sauzet, Gustavo Schwenkler, and participants at the HEC-McGill Winter Finance Workshop, the 11th FIRN Annual conference, and seminars at McGill and UTS. We thank Calcul Québec and Compute Canada for access to the supercomputer Cedar. Ericsson (corresponding author) is from the Desautels Faculty of Management at McGill University; e-mail: jan.ericsson@mcgill.ca. Glover is from UTS Business School; e-mail: kristoffer.glover@uts.edu.au. Jeanneret is from UNSW Business School; e-mail: a.jeanneret@unsw.edu.au; website: www.alexandrejeanneret.net. Lu is from the University of Melbourne FBE; e-mail: lucie.lu@unimelb.edu.au; website: www.yiliulu.com. All errors are our own.

Default Risk Linkages in a Structural Credit Model

ABSTRACT

This paper proposes a novel explanation for the linkages between the default risk of borrowers. A negative idiosyncratic shock to one borrower reduces its creditworthiness but also makes another borrower a relatively larger player in the economy, increasing the latter's systematic risk. Debt costs then increase for the second borrower, tilting its decision towards an earlier default. This effect strengthens with greater refinancing needs due to shorter debt maturity. Our model thereby generates positive co-movement in credit spreads, risk premia, and equity volatilities across fundamentally unrelated borrowers, providing novel insights into the interplay between credit and equity markets.

JEL classification: G12, G13, G32, G33.

Keywords: Credit Risk, Structural Models, Asset Prices, Leverage, Volatility, Spillovers.

The theoretical literature on credit risk has made significant strides since Merton's (1974) seminal work. It has helped us understand credit spreads, suggested a framework for assessing capital structure choices, enabled us to study the interplay between different sources of risk affecting equity and bond prices, and allowed us to evaluate derivatives in debt and equity markets. However, little has been done to examine the *linkages* between borrowers' default risk. Indeed, existing credit risk theory has concentrated on individual firms or large portfolios of atomistic firms, leaving us with limited knowledge about the impact of one firm's fate on the creditworthiness of others.

In this paper, we propose a new mechanism for endogenous default risk linkages in a multi-borrower economy and analyze its implications for asset pricing. Our primary objective is to understand how shocks to the fundamentals of one borrower, which could be a firm, industry, bank or sovereign, can have an impact not only on its own creditworthiness but also on other potentially uncorrelated borrowers. By doing so, we aim to explain the co-movement in default risk observed across these borrowers. To achieve our objective, we enrich a standard structural credit model with a multi-borrower setting. Specifically, we introduce debt and default risk into the two-tree equilibrium framework developed by Cochrane, Longstaff, and Santa-Clara (2008).[1]

Our first contribution is to reveal how a shock to one borrower impacts the default decisions of all borrowers, by way of fluctuations in equilibrium risk premia. This creates a new type of default risk linkage, which results in an economically significant level of *excess correlation*. In our baseline calibration, the correlation in default risk across borrowers is 9.5% higher than the correlation in their fundamentals.

We also find that the transmission of default risk across borrowers is amplified when refinancing is more imminent due to shorter debt maturity. Moving from perpetual to 5-year-maturity bonds, for example, increases the baseline excess correlation by 5.8% (to 15.3%). The reason for this increase is that a shock to one borrower affects the risk premium and thus the cost of debt refinancing of the other borrower, thereby increasing its default probability. Our second contribution is thus to highlight the unique role of refinancing needs in a multi-borrower economy, complementing recent work on refinancing risk in single-firm default decisions (see He and Xiong, 2012) and equity risk premia (see

[1] Clearly a two-tree economy is a stylized representation of reality. Nonetheless, the intuition we develop in this setting would be valid in a richer setting with more trees. However, one can also think about our model as one tree representing a borrower or portfolio of borrowers (e.g. an industry), while the second summarizes the rest of the economy.

Chaderina, Weiss, and Zechner, Chaderina et al.; Friewald, Nagler, and Wagner, 2022).[2]

Our third contribution is to show that the endogenous transmission of default risk across borrowers also has significant consequences for equity investors. We demonstrate that increased default risk across borrowers also results in higher leverage, leading to a positive co-movement in their equity risk premia and volatilities. This result is in contrast with the classic two-tree economy without leverage, where each tree's systematic risk moves in opposite directions, resulting in negative co-movement in equity expected excess returns and volatilities. Our findings are consistent with the empirical evidence presented by Herskovic, Kelly, Lustig, and Van Nieuwerburgh (2016, 2020) and thus contributes to a deeper understanding of the interplay between credit and equity markets in a multi-borrower economy.

The core intuition of our model, which we summarize in Figure 1, is as follows. When one borrower (B) experiences a negative shock to its fundamentals, reducing the value of its assets and increasing its default risk, the other borrower (A) represents a larger proportion of the economy and bears more systematic risk, as in Cochrane et al. (2008). The novelty of our paper is to show that, in the presence of leverage, the higher risk premium reduces borrower A's continuation value and skews its decision towards defaulting, even if its fundamentals remain unchanged. As a result, borrower A's default risk endogenously increases following a negative shock to the fundamentals of borrower B, causing positive co-movement in their default risk and credit spreads. This mechanism also applies to equity volatility through variation in the borrowers' leverage ratios.

Our model also highlights that the borrower's average debt maturity significantly influences these effects, as their default decision is directly impacted by the level of immediate refinancing needs. Specifically, the increased risk premium raises the borrower's cost of debt refinancing, exacerbating the rise in default risk. Rollover risk, therefore, amplifies a borrower's exposure to the fate of the other borrower.

FIGURE 1 ABOUT HERE

An additional important finding is that the excess default risk correlation remains robust and quantitatively similar across different tree sizes. This result effectively addresses the concern that the

[2]Other notable papers that consider refinancing risk in structural models include Leland and Toft (1996), Leland (1998), He and Milbradt (2014), Chen, Cui, He, and Milbradt (2018), Choi, Hackbarth, and Zechner (2018), and Dangl and Zechner (2021).

transmission of default risk could be relevant only for borrowers with large contributions to aggregate fluctuations. Moreover, we demonstrate theoretically that the co-movement in default risk is independent of the chosen debt level, which is a direct consequence of a scaling property relating to bond valuation (the optimal default boundary is a linear function of the debt coupon). Therefore, the default risk transmission mechanism we advance in our paper applies to both exogenous and endogenous financing policies and is a general mechanism that does not rely on a set of restrictive assumptions.

These theoretical findings have widespread implications for understanding recent developments in financial markets. For example, they offer new insights on the pivotal role of corporate bailouts in averting bankruptcy cascades during times of financial crises. Our main intuition regarding default risk linkages via changes in risk premia can indeed be viewed in reverse. During times of market stress, governments often provide direct credit and policy support to firms in need. However, determining which firms or sectors should receive the most aid can be controversial, as seen in the recent Covid-19 crisis.[3] Our model suggests that beneficial spillovers can result from government support to any sector. A wealth increase for firms in one sector effectively lead to a favourable repricing of other firms in the economy since the latter now bear less systematic risk. As a result, even firms that do not receive direct support can benefit from lower funding costs and reduced probability of default. Thus, a rescue package can improve the creditworthiness of all firms, regardless of their fundamental relationship to the sector receiving the bailout.

The mechanism we highlight in this paper is also relevant for understanding credit risk transmission in the sovereign debt market, where a default crisis in one country can have spillover effects on seemingly unrelated countries. A notable case is the events leading up to the Russian default in August 1998, which likely had a causal effect on the creditworthiness of other governments. This effect was particularly noticeable in the months leading up to the crisis, as bond spreads of countries with distinct geographical locations increased substantially. Our model helps explain this phenomenon, with the 1997-1998 decline in Russia's real GDP acting as an exogenous shock to the first borrower's fundamentals. As predicted by our model, the gradual widening in credit spreads for Brazil, for instance, is consistent with the increased risk premium for the second borrower.[4] Moody's downgrade

[3] See, for example, the articles "Who Should Get Bailed Out in the Coronavirus Economy?", published by the New Yorker on April 22, 2020, and "US Big Business Gets Help First but Who Needs it Most?", published by the Financial Times on May 26, 2020.

[4] In the context of international finance, each tree can be seen as a separate country, with country-level output

of Brazilian debt on September 3, 1999, further emphasizes the impact on Brazil's default probability. What is striking is that there were no strong fundamental links between Brazil and Russia, with their GDP growth rate correlation being –0.14 over the 1990–1998 period. Our model can thus be useful for understanding how default risk can spill over to sovereign borrowers that are fundamentally unconnected.

A third application of our rollover channel is to offer an explanation for the clustering of sovereign debt distress episodes during the European debt crisis in 2010-2012. Policymakers were particularly concerned about the potential spillovers in default risk from Greece, given the concentrated amount of government debt subject to imminent refinancing. The countries most severely hit during the crisis were generally those with the highest fraction of debt maturing within the following year. These countries, located in the southern periphery of Europe, had a refinancing schedule requiring more immediate short-term rollover than their northern counterparts. Our model suggests that the spillover in borrowing costs through bond risk premia, combined with high exposure to rollover risk, may have played an important role in the default risk transmission among southern countries, despite their weak economic ties.[5] This mechanism is consistent with the spillovers of sovereign credit risk for the Eurozone documented by Gabaix and Koijen (2022), among others.

The basic setup of our model is borrowed from Cochrane et al. (2008), which comprises two Lucas trees that represent the unlevered assets of borrowers with standard output dynamics. We then incorporate a credit model similar to Leland (1994) and Leland (1998). This setup enables us to derive the borrowers' endogenous default decisions, taking into account the amount of debt issued as well as its average maturity. Our model expands traditional structural credit models to an economy where two state variables, i.e., the borrowers' own output dynamics and their relative share in the economy, now drive asset valuations and default decisions. This way, we can examine the transmission of default risk within financial markets, which we will argue represents an additional layer to the previously studied contagion in asset prices. Notably, the transmission of default risk can sometimes reinforce the effects of Cochrane et al. (2008), such as in the case of equity valuation, but it can also counteract and dominate them, as evidenced by the co-movement of equity volatility.

shocks (e.g., Pavlova and Rigobon, 2007). The drop in the value of Russian government debt raised Brazil's default risk and increased its risk premium and rollover risk.

[5]For example, the overall value of bilateral trade between Greece and Portugal in 2010 was less than 300 million euros, negligible compared to their respective GDPs.

In order to isolate the default risk spillover effects, the benchmark scenario we set out relies on two borrowers with independent fundamentals. However, in practice, co-movement in default risk can result from borrowers being subject to common sources of fundamental shocks, as studied in Bao, Hou, and Zhang (2023).[6] We therefore extend our analysis to account for correlated output shocks, finding that positively correlated fundamentals reduce the variability of the risk-premium and mitigate default risk transmission. While co-movement in default risk and equity volatility may increase with more correlated fundamentals, the spillover effects we identify act as a substitute for fundamental correlation. Thus, our proposed mechanism may help explain why common factors alone cannot fully account for the degree of corporate default clustering (e.g., Das, Duffie, Kapadia, and Saita, 2007).

We acknowledge that a firm's default is also likely to have a *direct* impact on the creditworthiness of other firms, as demonstrated in studies such as Azizpour, Giesecke, and Schwenkler (2018).[7] However, our approach differs from these studies as it does not require a causal relationship between a borrower's default and the default probabilities of others. Our mechanism proposes an alternative source of default clustering, through market clearing, that does not rely on shared fundamentals or explicit contagion through default events.

In sum, our model can create spillover effects in both default risk, equity volatility, and risk premia through a single mechanism: the response of borrowers' default decisions to changes in equilibrium risk pricing. To the best of our knowledge, this is the first model that can generate such predictions in a unified framework.

This paper draws on insights from various strands of the asset pricing literature. First, we build on the extensive literature on structural credit models that has been developed based on Merton (1974). Specifically, we integrate equilibrium conditions into a model of borrower default and debt valuation, building on the framework proposed by Leland (1994) and Leland (1998). Our approach is related to a recent branch of the credit literature that has incorporated consumption-based asset dynamics into structural models, including studies by Chang and Sundaresan (2005), Chen, Collin-Dufresne, and Goldstein (2008), Bhamra, Kuehn, and Strebulaev (2010), and Chen (2010). In contrast to our

[6]Examples of such co-movement include those arising from aggregate cash flow shocks (Fudenberg and Maskin, 1986), financial network linkages (Allen and Gale, 2000), self-fulfilling beliefs (Goldstein and Pauzner, 2004), or competition across firms (Chen, Dou, Guo, and Ji, 2023).

[7]Other empirical studies have found that defaults can have spillover effects within industries (Lang and Stulz, 1992; Jorion and Zhang, 2007), through business connections (Jorion and Zhang, 2009), via networks of firms (Acemoglu, Ozdaglar, and Tahbaz-Salehi, 2015; Elliott, Golub, and Jackson, 2014), or through competition (Chen et al., 2023).

model, a key feature of this literature is that individual firms have no impact on the fate of others, and changes in asset value dynamics have only redistributive effects across claimants.

The second strand investigates asset prices in an endowment economy with a representative agent consuming the output of multiple trees. Cochrane et al. (2008) study the case of two Lucas trees, while Martin (2013) extend the model to a collection of trees (a Lucas orchard). In these models, a shock to the output of one tree affects the output shares and hence valuation ratios of all other assets.[8] However, in the absence of leverage, asset volatilities (and risk premia) tend to move in opposite directions, as an increase in one tree's systematic risk reduces the risk of other trees. In this paper, we highlight an endogenous response in default risk that reverses this negative volatility co-movement. Our findings are distinct from those of Hasler and Ornthanalai (2018), who demonstrate that investors' fluctuating attention to news can generate contagion in asset returns and volatilities when expected output growth is unobservable. Instead, we show that introducing debt in a Lucas tree economy with complete information can jointly generate positive co-movement in the risk premium, equity volatility, and default risk across borrowers. We further establish in a simulated economy that these effects are economically significant. For example, the mean correlation between equity volatilities (risk premia) across independent borrowers is 24% (38%).

Overall, this paper offers a unique contribution by departing from the traditional case of atomistic firms and instead studying how a shock to one firm can impact another firm in the economy through market clearing conditions. Unlike existing structural models for atomistic firms, where a borrower's default boundary is unaffected by the fate of others, the valuation of a borrower's assets and its default risk in this model depend on the market equilibrium resulting from changes to any borrower's fundamentals. By demonstrating that a shock to one borrower can impact another borrower's default risk, credit spread, equity volatility, and expected return, we highlight a new mechanism for default risk transmission that can help us understand stylized facts in credit and equity markets.

[8]Other related studies include Dumas (1992) and Pavlova and Rigobon (2007) for the two-country economy case, Menzly, Santos, and Veronesi (2004) for the predictability of returns in an equilibrium model with multiple securities and habit preferences, Santos and Veronesi (2010) on the cross-section of stock returns, Buraschi, Trojani, and Vedolin (2014) for an explanation of option prices in a Lucas orchard with investors' disagreement, and Sauzet (2022) for the case of two goods and heterogeneous preferences.

1 Model

We develop a model to study how endogenous variation in risk premia creates default risk linkages across borrowers. In our baseline version we embed a credit model with perpetual debt (Leland, 1994) in an equilibrium economy (Cochrane et al., 2008), where two Lucas trees make up the unlevered assets of the borrowers. This setting allows us to analyze how a borrower's endogenous default decision varies with its relative contribution to the economy. This model is subsequently extended in Section 3.1 with finite-maturity debt to investigate the additional effects of rollover risk. We first describe the economic environment, evaluate the assets of the borrowers, and then discuss the optimal default policy.

1.1 Environment

The economy consists of two Lucas trees ($i = A, B$), which can be viewed as two distinct borrowers. Each tree generates a stream of output that evolves according to

$$\frac{dX_t^i}{X_t^i} = \mu_i dt + \sigma_i dB_t^i, \tag{1}$$

where μ_i denotes the expected growth rate and σ_i is the volatility of tree i's output. The trees are subject to Brownian shocks dB_t^A and dB_t^B under the physical-probability measure, whose correlation is given by ρ. While our base case relies on independent trees, we consider the role of correlated shocks as an extension.

The output share, which captures the relative importance of the two trees, is a key state variable for this economy, as in Cochrane et al. (2008). The time-t output share of tree A, denoted by s_t, is determined by

$$s_t = \frac{X_t^A}{X_t^A + X_t^B}, \tag{2}$$

whose dynamics satisfy the process

$$\begin{aligned} ds_t &= s_t(1-s_t)\left[\mu_A - \mu_B - s_t\sigma_A^2 + (1-s_t)\sigma_B^2 + 2(s_t - 1/2)\rho\sigma_A\sigma_B\right]dt \\ &\quad + s_t(1-s_t)\left(\sigma_A dB_t^A - \sigma_B dB_t^B\right), \end{aligned} \tag{3}$$

such that the output share s_t increases (decreases) with unexpected shocks to tree A (B). Note that output share volatility is highest when the trees are of equal size and becomes zero when the economy converges to a single borrower.

A representative agent with log utility and time discount rate δ consumes aggregate output. The dynamics of aggregate consumption, given by $Y_t = X_t^A + X_t^B$, follow

$$\frac{dY_t}{Y_t} = [s_t\mu_A + (1-s_t)\mu_B]\,dt + s_t\sigma_A dB_t^A + (1-s_t)\sigma_B dB_t^B \tag{4}$$

$$\text{var}_t\left[\frac{dY_t}{Y_t}\right] = s_t^2\sigma_A^2 + (1-s_t)^2\sigma_B^2 + 2s_t(1-s_t)\rho\sigma_A\sigma_B, \tag{5}$$

which implies that the consumption growth variance, denoted by $\text{var}_t\left[\frac{dY_t}{Y_t}\right]$, is stochastic and peaks when $s_t = 0$ and $s_t = 1$ and is lowest for intermediate values of the output share, i.e., when consumption is most diversified between the two output sources.

The endogenous stochastic discount factor (SDF), equivalent to $e^{-\delta t}/Y_t$ and denoted by M_t, follows

$$\frac{dM_t}{M_t} = -r_t dt - s_t\sigma_A dB_t^A - (1-s_t)\sigma_B dB_t^B, \tag{6}$$

where r_t is the equilibrium risk-free rate given by

$$r_t = \delta + s_t\mu_A + (1-s_t)\mu_B - s_t^2\sigma_A^2 - (1-s_t)^2\sigma_B^2 - 2s_t(1-s_t)\rho\sigma_A\sigma_B, \tag{7}$$

which is stochastic and varies with the share s_t.

The SDF implies that the market prices of risk of the shocks to trees A and B correspond to $s_t\sigma_A$ and $(1-s_t)\sigma_B$, respectively. The price of risk of one tree thus increases with its relative contribution to aggregate consumption, as captured by s_t for A and $1-s_t$ for B.

1.2 Security valuation

We now analyze the pricing of the borrowers' levered equity and debt, thus departing from the unlevered case of Cochrane et al. (2008). Assuming the consol debt financing structure of Leland (1994) allows us to focus on the spillover mechanism in a parsimonious setting. However, we will

show that all qualitative results extend to a model with finite-maturity debt.

We assume each borrower issues perpetual debt with a fixed, tax deductible, coupon C_i.[9] Letting φ denote the borrower's tax rate, the levered equity value can be written as

$$E^i(X_t^i, s_t) = \sup_{\tau_i \geq t} \mathbb{E}_t \left[\int_t^{\tau_i} \frac{M_u}{M_t}(1-\varphi)(X_u^i - C_i)du \right], \tag{8}$$

where τ_i is the random time at which the borrower i defaults on its debt obligations. We will show that default occurs when output X_t^i falls to an endogenous stochastic boundary $b_{i,t}$, which will depend on the output share s_t. This is because there are two key factors influencing the valuation of a borrower's equity and hence the default decision. One is the level of the risk-free rate, which changes in lockstep with the output share. The second is the market price of risk of the aggregate output shocks, which also varies with the output share.

Note that in the absence of debt, when $C_i = 0$, Equation (8) respresents the unlevered asset value of each tree, i.e. the present value of all future cash flows discounted using the common stochastic discount factor. Denoting this unlevered value as U^i we have

$$\begin{aligned} U^i(X_t^i, s_t) &= \mathbb{E}_t \left[\int_t^{\infty} \frac{M_u}{M_t}(1-\varphi) X_u^i du \right] \\ &= (1-\varphi)\mathbb{E}_t \left[\int_t^{\infty} e^{-\delta(u-t)} \frac{Y_t}{Y_u} X_u^i du \right] \\ &= (1-\varphi) X_t^i V^i(s_t), \end{aligned} \tag{9}$$

where the function $V^i(s_t)$ can be obtained in closed-form.[10]

Turning to the valuation of debt, we assume that, upon default, creditors recover a fraction $1-\epsilon$ of the value of the unlevered assets of the tree backing their claim, leaving the borrower's residual claimants with nothing. In other words, a fraction ϵ of the unlevered asset value is lost in the bankruptcy process.[11] The value of debt can therefore be expressed as

[9] We can consider an exogenous financing policy because we will prove that our main results are independent of the chosen debt level (Section 2.4).

[10] Cochrane et al. (2008) provide a closed-form solution for the function $V^i(s_t)$, representing the price-to-dividend (output) ratio of the tree in their unlevered model (see Equation A.1). This expression involves a set of hypergeometric functions that can be evaluated numerically.

[11] We extend our model to investigate the effect of alternative default assumptions in Appendix C.1. Note, however, that taxes and bankruptcy costs have no effect on aggregate consumption and the SDF in the economy. Corporate taxes are composed of transfers redistributed (by a benevolent government) to the representative agent, while bankruptcy costs can be viewed as (lawyer) fees paid to the agent to restructure the defaulting firm. One way to view this is that

$$D^i(X_t^i, s_t) = \mathbb{E}_t \left[\int_t^{\tau_i} \frac{M_u}{M_t} C_i du + \frac{M_{\tau_i}}{M_t}(1-\epsilon) U^i(X_{\tau_i}^i, s_{\tau_i}) \right], \tag{10}$$

such that the credit spread of newly-issued debt is given by

$$CS_t^i = \frac{C_i}{D^i(X_t^i, s_t)} - y_t, \tag{11}$$

where y_t is the yield on a risk-free bond that accounts for the stochastic nature of the (instantaneous) risk-free rate r_t.

A novel aspect of our model is that the optimal default policy is endogenously time-varying, as it now depends on the output share s_t. This is in contrast to most structural models à la Leland (1994), whereby the default boundary is time-invariant, as it depends on the debt level, asset volatility, and the risk-free rate, among others, which are all assumed to be constant. Yet, the intuition for the default decision is very much the same as in Geske (1977) and Leland (1994): shareholders trade off the cost of avoiding default (servicing debt) and the continuation value of equity (future upside).[12] The added technical difficulty is that the continuation value of a borrower now depends on two state variables: the dynamics of its own output and the relative share of the borrower in the economy.

One technical contribution of the paper is to propose a numerical solution (via finite-difference methods) of the associated set of (free-) boundary-value problems. We solve for the equity and debt values via partial differential equations (PDE), rather than via simulation. The advantage of the PDE approach is that it allows us to solve for all values of the output share s_t simultaneously, rather than running a separate simulation for each separate output share. Our PDE methodology also allows us to exploit the existence of closed-form expressions for security values in the limit as the output share approaches zero (with tree A becoming atomistic) and in the limit as the share approaches one (corresponding to a single tree economy). The details of the solution method are discussed in Appendix A.

---

the Modigliani Miller irrelevance result applies to the value of the sum of the two unlevered trees. Any changes in taxes, bankruptcy costs, equity and debt are merely redistributive.

[12] We can also express the criterion for default as follows: for a given output share, shareholders seek to keep the borrower solvent until the lowest possible (own) output level consistent with limited liability.

2 Predictions

In this section, we highlight a new source of default risk co-movement that arises in a Lucas economy with two levered, independent trees. We begin by reviewing key market equilibrium effects and their implications for equity and debt valuation. We then analyze how a borrower's creditworthiness depends on shocks affecting another borrower, thereby generating co-movement in their default risk. After this, we discuss the role of this risk transmission for credit spreads and highlight how this mechanism can generate new insights on the co-movement in equity volatility and risk premia across borrowers.

2.1 Calibration

We set the parameters of our two-tree economy as follows. The expected growth rates of trees A and B are $\mu_A = \mu_B = 0.02$ and their volatilities are equal to $\sigma_A = \sigma_B = 0.2$, in line with Cochrane et al. (2008). In the base case, the trees are independent (i.e., $\rho = 0$), but we relax this assumption in Section 3.2. The time discount rate is set to $\delta = 0.06$. The tax rate is set to 15% (i.e. $\varphi = 0.15$) and we assume that 37.8% of the unlevered asset value are recovered in bankruptcy (i.e. $\epsilon = 0.622$), as in Feldhütter and Schaefer (2018) and Bai, Goldstein, and Yang (2020). Unless otherwise stated, we normalize the initial output levels to one, i.e., $X_0^i = 1$. The baseline debt coupon is set to $C_A = C_B = 0.4$, but we also consider lower ($C_i = 0.2$) and higher ($C_i = 0.6$) debt levels to generate predictions across book leverage. The set of parameter values is summarized in Table 1.

TABLE 1 ABOUT HERE

Under the benchmark calibration ($s_t = 0.5$), leverage, credit spreads and equity return volatility of tree A are 41.8%, 80bps, and 29.2%, respectively. Huang and Huang (2012) report an average leverage of 43.28% for Baa firms, while Kang and Pflueger (2015) report 41%. The average credit spreads for long maturity bonds is 82 bps in Davydenko and Strebulaev (2007), while Bhamra, Dorion, Jeanneret, and Weber (2023) report an average equity volatility of 33.15%. In addition, the (levered) equity risk premium equals 3.18%, which compares to the level (3.22%) obtained in a structural model

with macroeconomic risk (Bhamra et al., 2010). The model-implied moments are thus reasonably close to their empirical counterparts.

2.2 Equilibrium asset prices

We first review how aggregate risk, the risk-free rate, and asset prices vary in equilibrium with fluctuations in the size of the trees. We consider variations in the relative size of tree A, denoted by the share s_t, that arise exclusively from idiosyncratic shocks to tree B. That is, we keep tree A's output constant to avoid a mechanical variation in this tree's creditworthiness. Our intent with this exercise is to ask what an exogenous shock to one borrower's fundamentals implies for the asset valuation, default decision, and creditworthiness of another borrower whose fundamentals remain unchanged.

2.2.1 Aggregate risk, risk-free rate, and equity valuation

We start by illustrating two standard features of the two-tree economy, discussed in Cochrane et al. (2008), but which are going to play a critical role for understanding default risk: i) Consumption growth volatility is a convex quadratic (U-shaped) function of the share s_t. It is thus lowest for equal values of the output share ($s_t = 0.5$), that is when consumption is the most diversified; ii) The risk-free rate, which varies negatively with such volatility through the precautionary savings motive, is the mirror image and thus inherits a hump shape. These equilibrium effects are illustrated in Panels A and B of Figure 2.

FIGURE 2 ABOUT HERE

Another central feature of Cochrane et al. (2008) that echoes in our model is how shocks to one tree induce variation in systematic risk. Fundamentally, the level of systematic risk of a tree increases with its contribution to the economy, as a tree with a larger share is less desirable from a diversification perspective. So if a negative shock hits tree B, investors want to rebalance and reduce their wealth across both trees. However, as investors cannot simultaneously rebalance all portfolios, given that the assets are in fixed supply, prices and expected returns must adjust. As the size of tree B shrinks, investors find it attractive to hold a smaller share of tree B. In contrast, the risk premium of tree A

must then increase (Panel C) and its equity valuation fall (Panel D), so that investors are willing to hold it in higher proportion. In equilibrium, a shock to one tree affects the other's asset valuation, creating contagion in asset prices, even in the absence of a common source of risk.

2.2.2 Debt valuation and leverage

We now discuss how these equilibrium effects drive a borrower's debt valuation and leverage, which are novel aspects of our model. The relationship between tree A's debt value and its contribution to aggregate fluctuations, as measured by the output share s_t, is a combination of two effects. First, as the share of tree A increases (following a negative shock to tree B), the higher risk premium reduces the value of its debt, which creates a negative relationship between debt valuation and the output share. Second, debt valuation is inversely related to the risk-free rate, which creates a U-shaped relationship between debt valuation and the output share. Panel E of Figure 2 illustrates the combined effect.

In sum, both equity and debt prices fluctuate endogenously with the relative importance of a borrower in the economy. However, we find that the effect on debt valuation differs qualitatively from the effect on equity valuation, which implies that leverage (debt value over the sum of debt plus equity values) varies non-trivially in equilibrium. We can indeed see that, when a borrower becomes a relatively larger player in the economy, its leverage tends to increase (Panel F), although the fundamentals of this borrower do not change. This points towards an increase in default risk in response to negative shocks hitting the other borrower. This transmission in default risk across borrowers, which we discuss in more detail below, is the focus of this paper.

2.3 Default risk linkages across independent borrowers

In this section, we discuss how an economy with two levered trees can experience endogenous default risk linkages across borrowers. By default risk linkages, we have in mind an increase in the (physical) default probability of one borrower (A) due to a negative shock to another borrower (B)'s fundamentals, whose default risk also increases. Specifically, we show that as borrower A becomes a greater player in the economy, given that the size of borrower B shrinks, the increased risk premium of borrower A skews its decision towards defaulting, although its fundamentals remain the same. Default

risk thus co-moves across the two borrowers, despite their independent fundamentals.[13]

2.3.1 Endogenous default decision

We first explore the predictions for a borrower's default policy, as characterized by its optimal default boundary $b_i(s_t)$. We can then measure (physical) default risk with the distance-to-default, defined as the log distance between a tree's output level and the corresponding default boundary, normalized by its output volatility. The distance-to-default for tree i is then $DD_t^i = \frac{1}{\sigma_i} \ln\left(\frac{X_t^i}{b_i(s_t)}\right)$. In our setting, the output volatility is constant, which implies that any increase in the boundary is equivalent to a decrease in the distance-to-default, i.e., the borrower is more likely to default. Similarly, when the output of a tree approaches its endogenously determined default boundary, the distance-to-default decreases and default risk increases. Given its simplicity, the distance-to-default is widely used in practice, being a useful default predictor in reduced form credit models (e.g., Duffie, Saita, and Wang, 2007; Bharath and Shumway, 2008; Campbell, Hilscher, and Szilagyi, 2008).

To understand the mechanism linking default risk across borrowers in our model, consider a negative (idiosyncratic) shock to tree B, while keeping the output of tree A unchanged, i.e., a decline in the share of tree B. Clearly, this negative shock leads to a deterioration in the fundamentals of tree B, which translates into a lower distance-to-default and, thus, creditworthiness.

The more interesting effect is what happens to tree A. In relative terms, tree A becomes a greater contributor to aggregate consumption and, thus, exhibits higher systematic risk. The increase in risk premium for tree A reduces the present value of future cash flows to equity, and as a result, decreases the option value of waiting to default. This effect appears in the form of a higher optimal default boundary, as illustrated in Panel A of Figure 3, and thus a lower distance-to-default. Tree A is then more likely to default on its debt when it becomes a greater player in the economy, as a result of tree B being hit by a negative shock. In contrast, a positive shock to tree B decreases the share of tree A, reduces its risk premium and, and then its default risk. Tree A's creditworthiness thus directly depends on the fate of tree B.

FIGURE 3 ABOUT HERE

[13] This is reminiscent of what is known in the literature as *default contagion*, where the default of one borrower can cause the default of another. However, in our model the default event is not a driver of another's default, rather default risk will co-move across borrowers through contagion in risk premia and the resulting impact on default decisions.

2.3.2 Co-movement in default risk

A direct implication of this mechanism is co-movement in default risk across borrowers, as their distances-to-default move in tandem when one borrower experiences a shock while the other does not. An economy with two levered trees features endogenous co-movement in default risk and, thus, a potential clustering of defaults, even when their fundamentals are independent. The primary transmission channel arises from a borrower's default policy varying endogenously with equilibrium risk premia. We thus point to a new mechanism through which market clearing conditions can generate real effects, by inducing a transmission in default risk from one borrower to another. This is a unique prediction of our two-tree economy with debt. Thus far, existing models with multiple unlevered trees (e.g., Pavlova and Rigobon, 2007; Cochrane et al., 2008; Martin, 2013; Hasler and Ornthanalai, 2018) have abstracted from default risk, while credit risk theories based on Leland (1994)'s model have focused exclusively on individual firms or portfolios of atomistic firms. Our contribution is to combine these distinct strands of literature and to show how shocks to one borrower can increase the default risk of another fundamentally-independent borrower.

To provide more quantitative insight into the co-movement in default risk between borrowers, we compute the correlation between their distances-to-default, given the stochastic fluctuations in both the output process X_t^i and the default boundary $b_i(s_t)$. Specifically, we have:

PROPOSITION 1. *Define the distance-to-default for tree i to be $DD_t^i = \frac{1}{\sigma_i}\ln\left(\frac{X_t^i}{b_i(s_t)}\right)$, where X_t^i and s_t follow the dynamics in* (1) *and* (3)*, respectively. The correlation between the changes in distance-to-default across borrowers, $\rho_{DD}(s_t) := \text{Corr}\left(dDD_t^A, dDD_t^B\right)$, is*

$$\rho_{DD}(s_t) = \frac{\rho[(1 - f_A(s_t)f_B(s_t)] + \alpha_A f_A(s_t) - \alpha_B f_B(s_t)}{\sqrt{[1 + 2\rho\alpha_A f_A(s_t) + \alpha_A^2 f_A^2(s_t)][1 - 2\rho\alpha_B f_B(s_t) + \alpha_B^2 f_B^2(s_t)]}}, \tag{12}$$

where $\alpha_i := \sigma_{-i}/\sigma_i$ and

$$f_i(s_t) := s_t(1 - s_t)\frac{b_i'(s_t)}{b_i(s_t)}, \tag{13}$$

which represents the sensitivity of tree i's default boundary b_i to changes in output share s_t.

Proof. See Appendix B. □

COROLLARY 1. *Letting* $\rho = 0$ *in* (12) *yields*

$$\rho_{DD}(s_t) = \frac{\alpha_A f_A(s_t) - \alpha_B f_B(s_t)}{\sqrt{[1 + \alpha_A^2 f_A^2(s_t)][1 + \alpha_B^2 f_B^2(s_t)]}} > 0. \tag{14}$$

Given that the default boundary $b_A(s_t)$ is increasing in s_t (the share of tree A), we observe from (13) that $f_A(s_t) > 0$. Moreover, since the share of tree B is simply $1 - s_t$, we observe that $b_B(s_t)$ is decreasing in s_t and hence $f_B(s_t) < 0$. The correlation between the distance-to-defaults of the two trees is therefore positive, even when shocks to their output are independent ($\rho = 0$).

The level of this default risk correlation is economically meaningful. Our baseline calibration implies $f_A(0.5) = -f_B(0.5) \approx 0.0476$, which yields $\rho_{DD} \approx 9.51\%$ when $s_t = 0.5$. We stress that this correlation is between fundamentally *independent* borrowers, hence we can interpret this correlation as an *excess* co-movement in default risk caused by the mechanism outlined in this paper.[14] Recall that we consider the log utility case, so this excess correlation can be viewed as a lower bound: higher risk aversion would magnify variations in risk premia and thus strengthen the transmission of default risk across borrowers.

Importantly, the level of default risk correlation remains sizable and robust to variation in the output share s_t, as illustrated in Panel A of Table 2. That is, the default risk co-movement obtained in equilibrium applies equally to relatively small and large firms. This alleviates the concern that the transmission in default risk we identify only matters for borrowers contributing the most to aggregate economic fluctuations.

We also verify that this prediction remains robust to changing our assumption about *who receives what* in default (see Appendix C.1). Panel B of Table 2 shows that similar co-movement in default risk arises when shareholders and debtholders play a Nash bargaining game in default, as in Fan and Sundaresan (2000). In addition, we find that the degree of default risk co-movement only varies marginally with a borrower's characteristics (see Appendix C.2). Our prediction therefore does not hinge on a specific model calibration.

TABLE 2 ABOUT HERE

[14] As we will show later, the level of (excess) default risk correlation increases for borrowers with shorter-maturity debt (Section 3.1) and negatively-related output (Section 3.2).

2.4 Capital structure independence

Our analysis so far assumes an exogenous debt level, determined by the coupon C_i. In doing so, we intentionally abstract from an optimal financing policy. We now demonstrate that the co-movement between borrowers' default risk, as measured by the correlation in (12), is actually independent of a borrower's capital structure choice.

We see from (8) that equity values satisfies the following symmetry due to the multiplicative nature of geometric Brownian motion:

$$E(X_t^i, s_t; C_i) = C_i E\left(\frac{X_t^i}{C_i}, s_t; 1\right) \tag{15}$$

and hence $b_i(s_t; C_i) = C_i b_i(s_t; 1)$, i.e. the optimal default boundary scales linearly with the debt coupon C_i. This scaling property, which is shared with most Leland (1994)-type of models, is illustrated by Panel B of Figure 3, where each of the three boundaries for different C_i are merely scaled multiples of each other.

A novel implication of this scaling property is that $f_i(s_t)$, as defined in (13), is independent of C_i, so that the correlation $\rho_{DD}(s_t)$, as defined in (12), does not depend on the capital structure chosen by borrowers. Appendix D provides a proof and more details on this independence.[15] This fundamental result implies that there is no additional insight to be gained from endogenizing borrowers' leverage when the objective is to understand default risk co-movement.

2.5 Default probabilities

Until now, we have considered the distance-to-default as our key measure of default risk. The distance-to-default has the advantage of allowing its correlation across two trees to be computed in closed form. We now consider the default probability, which is perhaps a more intuitive metric.

Figure 4 illustrates how the default probabilities for the two borrowers behave as a function of the output share under both the physical and risk-adjusted measures. The difference between the two measures of default probability identifies the risk premium associated with default risk.[16] We report

[15] The extended version of our model with finite maturity debt exhibits the same symmetry.

[16] We compute the default probabilities via PDEs, using the methodology described in Appendix F. The 10-year default probability is within the confidence intervals reported in Feldhütter and Schaefer (2018) for a BBB firm. We calibrate the full term structure of default probabilities to study a simulated economy in Section 2.8.

predictions for the output share of tree A varying between 0.2 and 0.8 because tree B is in default outside of this range. The wedge between risk-neutral ($\mathbb{Q}$) and physical ($\mathbb{P}$) probabilities, measured as a ratio, varies between 1.43 (at $s = 0.2$) and 2.56 (at $s = 0.8$), which is consistent with the ratios of risk-neutral to physical default intensities reported in Driessen (2005) for BBB firms. Note that the ratio (and the difference) between $\mathbb{Q}$ and $\mathbb{P}$ in our model increases with the output share of tree A, so it is strongly tied to the level of systematic risk.

FIGURE 4 ABOUT HERE

We find that borrower A's physical default probability responds to a shock to borrower B and that the model also generates co-movement in probabilities across the two borrowers. In addition, the risk-adjusted default probability of tree A is even more responsive to a shock on tree B, which implies an increasing risk premium. This result should translate into a particularly strong co-movement in credit spreads and asset pricing moments, given they are derived under the risk-adjusted measure. In the next section, we explore the predictions for equilibrium credit spreads, which combine information about both the probability of default and risk premia.

2.6 Equilibrium credit spreads

It is particularly interesting to study credit spreads because a negative shock to borrower B affects credit spreads through two channels: a change in *level* of default risk and a change in the *price* of risk. To understand the two channels driving credit spreads, consider, as before, a negative shock to borrower B. As borrower A contributes more to the economy, the increase in its risk premium tilts that borrower towards increasing its optimal default boundary. The resulting increase in credit spread can be viewed as a 'quantity of default risk' effect. In addition, the higher risk premium implies a direct increase in the credit spread, which can be viewed as a 'price of risk' effect.

The combination of the two effects induces the credit spread of borrower A to increase with the relative size of this borrower in the economy, as illustrated in Panel A of Figure 5. Note that the exposure of borrower A's credit spreads to shocks impacting borrower B now increases with the level of leverage, although the sensitivity of the distance-to-default does not (given the scaling property

discussed in Section 2.4). This is because a shock to one borrower impacts the other borrower's credit spread by affecting *both* its default risk and its (levered) risk premium, which naturally increase with leverage.

In contrast, the effect on borrower B's credit spread is ambiguous because the two channels now work in opposite directions: while borrower B's negative shock increases its default risk, the level of systematic risk decreases and so does its risk premium. Yet we find that the default risk effect dominates the price of risk channel, that is, borrower B's credit spreads move in the same direction as borrower A's (see Panel B of Figure 5). This results in a co-movement in credit spreads across independent borrowers, complementing the co-movement in default risk discussed earlier.

FIGURE 5 ABOUT HERE

2.7 Co-movement in equity volatility and risk premia

Another important feature of financial markets is the co-variation in the equity volatility between fundamentally unrelated firms, which has been extensively documented in the empirical literature.[17] We now show that our model can explain a positive co-movement in equity volatility (and risk premia) through the endogenous default risk channel, without assuming any change in output volatility.[18] This result is not trivial because the offsetting variations in systematic risk across the two borrowers would generate a negative co-movement in equity volatility and risk premia in the absence of leverage and default risk.

To understand this mechanism, consider a negative shock to borrower B. The equity volatility of borrower A increases with its output share, as illustrated in Panel A of Figure 6. This result arises because the optimal default boundary increases with the level of systematic risk (borrower A becomes relatively larger), thereby increasing leverage and thus the level of equity volatility. Turning to borrower B, this shock increases that borrower's leverage, as its output approaches the default boundary, and thus its equity volatility, as displayed in Panel B of Figure 6. We can see that the positive effect of leverage on the equity volatility of borrower B dominates the decrease in equity volatility due to

[17] See, for example, Hamao, Masulis, and Ng (1990), Boyer, Kumagai, and Yuan (2006), Bekaert, Ehrmann, Fratzscher, and Mehl (2014), and Hasler and Ornthanalai (2018).

[18] Appendix E derives these equity return moments in our model.

the reduction in systematic risk (borrower B becomes relatively smaller). Shocks to one borrower thus generate co-movement in equity volatility across independent debt-financed trees. Similarly, we observe a positive co-movement in equity risk premia, as illustrated in Figure 7.[19]

FIGURES 6 AND 7 ABOUT HERE

These predictions stand in contrast to the case of unlevered trees, such as in Cochrane et al. (2008): an increase in the output share of one tree decreases that of the other, causing equity volatilities and risk premia to move in opposite directions across trees, as illustrated in Panels C and D of Figures 6 and 7. The mechanism is described in Figure 8. Such a counterfactual negative co-movement highlights the importance of considering debt financing. The default risk transmission that we document in this paper reverses the negative linkages in equity risk premia and volatilities and, as a result, generates predictions that are consistent with the positive co-movement observed in the data (e.g., Herskovic et al., 2016).[20]

FIGURE 8 ABOUT HERE

Our model can thus create spillover effects in both default risk, equity volatility, and risk premia through a single mechanism: the response of borrowers' default decisions to changes in equilibrium risk pricing. To the best of our knowledge, this is the first model that can generate such predictions in a unified framework.

2.8 Quantifying co-movement with simulated economies

So far, we have illustrated how our model implies co-movement among several metrics such as the default risk, leverage, credit spreads, risk premia, and equity volatilities. We now seek a better sense of the economic magnitude of such co-movements.

[19] Equity risk premia co-move positively when borrower B's default risk is high (when its output share is low, due to negative shocks), as the leverage channel dominates the change in systematic risk. In contrast, the leverage effect is weak when borrower B's default risk is low, so that the co-movement in risk premia becomes similar to the unlevered case.

[20] Hasler and Ornthanalai (2018) show that spillovers in return and volatility can also arise in a two-tree economy in which the representative investor needs to estimate unobservable expected output growth. Their incomplete information model abstracts from the leverage channel, whereas our model introduces debt financing in an economy without learning. Both mechanisms complement one another as means of understanding commonality in returns and volatility in financial markets.

To do so we simulate a dataset of multi-borrower economies and compute the correlations across trees. In contrast to model results discussed thus far, which are calculated for borrowers with output levels maintained at the level of bond issuance ($X_i = 1$), each simulated economy consists of borrowers endowed with different levels of output X_i and hence default risk. The simulation thus generates a panel of economies in which borrowers' default risk, credit spreads, and asset pricing moments display large variation both in the cross-section and time series. Appendix G describes the simulation procedure, based on 20,000 two-tree economies at the daily frequency over a 10-year period. The level and the term structure of default probabilities in our simulation exercise closely matches the empirical counterparts, as the 1-, 5-, and 10-year default probabilities are $1.41\%, 6.29\%$, and 11.79% in the simulation and respectively $1.86\%, 7.72\%$, and 11.37% in the data, based on the cumulative default rates for all-rated corporate bonds in the U.S. from Standard and Poor's (2021). Table 3 reports the sample correlation across trees, averaged across simulations, for different default risk measures in Panel B and asset pricing moments in Panel C.

TABLE 3 ABOUT HERE

We first notice that the correlations obtained from the distance-to-default and the 10-year cumulative default probability are quite similar, at 10.06% and 10.84% respectively. While the default probability and its correlation across borrowers may be more straightforward to interpret, considering the distance-to-default allows us to obtain a closed-form solution for its correlation with similar quantitative predictions. The correlations based on leverage ratios, however, show a slightly higher average value of 14.84%.

Default probabilities, distances-to-default, and leverage speak to the quantity of but not the pricing of default risk. The credit spread, on the other hand, combines the quantity and price of risk. We see in Table 3 that the average correlation for credit spreads is in fact higher, at 28.08%, than that for all three physical measures of default risk.

Next, we explore correlations in other asset pricing moments. Equity volatility, which would be negatively correlated across trees in the absence of financial leverage, exhibits a positive correlation of about 24%. An interesting observation is that the correlations become more pronounced when examining equity risk premia across borrowers, with an average correlation of about 38%. Additionally,

correlations based on debt risk premia and volatility (derived in Appendix E) exhibit a similar pattern, with even higher levels. The large correlations in debt moments across trees are largely due to the case when both borrowers become highly creditworthy, whereby fluctuations in debt values mostly reflect common variation in aggregate risk and the risk-free rate.

Finally, it is useful to compare the simulation outcomes of our model, consisting of an economy of two borrowers featuring stochastic default boundaries, with a scenario where the default boundaries remain constant. This counterfactual case can be viewed as two separate economies of one borrower each, whereby the default boundary of a borrower is independent of the fate of the other. We describe this analysis in Appendix G.2. Figure A.1 (A.2) plots the distributions of the correlation in default risk (asset moments) across trees for both cases. Notably, the average correlation level in our baseline model is clearly shifted towards the right of the distribution obtained in the counterfactual case. This result confirms that the strong co-movement revealed in Table 3 cannot be due to chance. Hence, this simulation exercise effectively demonstrates that the co-movement levels across trees, concerning default risk and asset pricing moments, are not only economically substantial but also statistically meaningful.

2.9 Summary

Our analysis has highlighted a new form of default risk transmission, where market clearing conditions can generate real effects: contagion in asset prices impacts borrowers' default policies and thus their default risk. We have shown that physical default risk can co-move positively across borrowers, even in the case of uncorrelated fundamentals. A direct implication of this mechanism is co-movement in credit spreads, equity volatility, and risk premia across borrowers. Our theory thus provides new testable predictions, both in the cross-section and time series, that can be tackled in future empirical research.

3 Extensions

This section provides several theoretical extensions. First, we relax the assumption of perpetual debt, allowing borrowers to issue finite maturity debt with a given rollover structure. All of the model's qualitative features carry over to such an extension, with the additional insight gained that

shorter maturity debt (i.e., the presence of higher rollover risk) increases the co-movement in default via the risk-premia channel. We then investigate how our findings vary when allowing for correlated fundamentals across trees.

3.1 A finite-maturity debt structure

Incorporating the financing structure of Leland (1998) allows us to nest the consol debt model considered in our baseline model, while also studying the consequences of short-term debt on rollover risk and, subsequently, the transmission of shocks from one tree to another. This extended version of the model shows that rollover risk and leverage interact with each other in modulating a borrower's default decision. Specifically, a borrower with shorter average debt maturity is more susceptible to experiencing large changes in default risk when another borrower is hit by a shock.

A number of papers on rollover risk find that the liquidity of the bond market matters for asset prices and thus for a borrower's endogenous default policy (see, e.g., Ericsson and Renault, 2006; He and Xiong, 2012; He and Milbradt, 2014). The complementary focus of our model is to explore how debt rollover risk amplifies the default decision of borrowers that is shaped by variation in equilibrium risk premia.

3.1.1 Rollover debt structure

We assume that each borrower issues a menu of bonds with different maturities and commits to rolling over this debt so as to keep the total face value P_i and coupon C_i constant. To maintain a stationary debt structure, borrowers continuously roll over a fraction m_i of total debt, which corresponds to the fraction of debt arriving at maturity. Hence, in every time interval $(t, t+dt)$, borrowers pay back $m_i P_i dt$ in maturing debt and replace it with newly issued debt with (equal) face value $p_i dt$, equal seniority, and equal maturity schedule. Hence $p_i = m_i P_i$. Given all debt has equal seniority, we assume that borrowers default on all debt simultaneously, at time τ_i. As in the baseline model, default occurs when the output X_t^i falls to an endogenous boundary $b_{i,t}$ that depends on the relative output share s_t.

In this extended version, rollover risk arises when a maturing bond is replaced by a new bond with equal coupon and principal. In contrast to the originally issued bond that is redeemed at par,

the new bond may not sell at par. Hence, if the borrower's fortunes take a turn for the worse, the proceeds of the refinancing may not cover the cost of paying off the maturing bond. When this happens, borrowers must make up the difference by injecting new funds, and this additional burden will influence their default decision.

3.1.2 Security valuation

This rollover structure ensures that at all points in time the borrower has current debt with an exponentially decaying remaining principal (with parameter m_i). Therefore, the *average maturity* of debt is given by $1/m_i$, and the total value of debt (at time t) is computed as

$$D^i(X_t^i, s_t) = \int_0^\infty e^{-m_i T} p_i d^i(X_t^i, s_t; T) dT, \tag{16}$$

where $d^i(X_t^i, s_t; T)$ denotes the (time-t) value of \$1 face value of debt, with a coupon rate c_i, maturing in T years' time, which is given by

$$\begin{aligned} d^i(X_t^i, s_t; T) = c_i \mathbb{E}_t \left[\int_t^{t+T} \frac{M_u}{M_t} I_{\{\tau_i > u\}} du \right] + \mathbb{E}_t \left[\frac{M_{t+T}}{M_t} I_{\{\tau_i > t+T\}} \right] \\ + \frac{(1-\epsilon)}{P_i} \mathbb{E}_t \left[\frac{M_{\tau_i}}{M_t} U^i(X_{\tau_i}^i, s_{\tau_i}) I_{\{\tau_i \leq t+T\}} \right]. \end{aligned} \tag{17}$$

The first term in (17) is the discounted expected value of the coupon flow, the second term represents the expected discounted value of repayment of the \$1 principal, while the third term reflects the expected discounted value of the tree's assets that bondholders recover upon default; where $1/P_i$ denotes the share of the total face value of debt of the \$1 bond (due to assumed equal priority).

Substitution of (17) into (16) yields the following expression for the total value of debt (see Appendix H.1):

$$D^i(X_t^i, s_t) = \mathbb{E}_t \left[(C_i + m_i P_i) \int_t^{\tau_i} e^{-m_i(u-t)} \frac{M_u}{M_t} du + e^{-m_i(\tau_i - t)} \frac{M_{\tau_i}}{M_t} (1-\epsilon) U^i(X_{\tau_i}^i, s_{\tau_i}) \right] \tag{18}$$

such that the total required annualized debt service equals the total coupon C_i $(= c_i P_i)$ plus the fraction of total principal P_i rolled over in a given year, $m_i P_i$. The corresponding credit spread is given

by

$$CS_t^i = \frac{C_i + m_i P_i}{D^i(X_t^i, s_t)} - y_t(m_i), \tag{19}$$

where $y_t(m_i)$ is the yield on a maturity-matched risk-free bond.

Turning to the valuation of equity, we recall that the debt structure described above exposes borrowers to rollover risk. Borrowers will face a cash shortfall if the newly-issued debt is priced below par, i.e. $D^i(X_t^i, s_t) < P_i$. Given that a fraction m_i of debt is rolled over at every instant, the net cash flow over the interval $(t, t + dt)$ is given by $m_i(D^i(X_t^i, s_t) - P_i)dt$. Hence, the value of equity solves

$$E^i(X_t^i, s_t) = \sup_{\tau_i \geq t} \mathbb{E}_t \left[\int_t^{\tau_i} \frac{M_u}{M_t} \left[(1-\varphi)(X_u^i - C_i) + m_i(D^i(X_u^i, s_u) - P_i) \right] du \right], \tag{20}$$

which implies that the degree of rollover risk will affect the optimal default policy of the firm, as any cash shortfall must eventually be financed by shareholders.

Note that the value of debt enters directly into the borrower's valuation problem in (20), and the borrower's optimal default decision (τ_i) enters into the debtholders' valuation problem in (18), so the two problems are *coupled* in a way that they are not with perpetual debt. Appendix H provides details of the solution to the system (18)+(20) via the numerical solution of associated boundary-value problems.

3.1.3 Calibration of the additional parameters

We use the same calibration as described in Section 2.1, with the following additional assumptions regarding the rollover debt structure. First, in our baseline parameterization, we set the average debt maturity equal to 10 years, which corresponds to $m_i = 1/10$. We also consider shorter (5 years; $m_i = 1/5$) and longer (30 years; $m_i = 1/30$) debt maturities to generate predictions for different degrees of rollover risk. Second, for each bond, we calibrate the principal such that it equals the value of a perpetual risk-free bond, i.e., $P_i = C_i/r_t$ using the risk-free short rate obtained when both trees have equal output shares (i.e., $s_t = 0.5$).[21] In the case of 10-year maturity debt, leverage, credit spreads and equity return volatility of tree A increase to 45.4%, 107bps, and 35.6%, respectively. These values remain similar to what is found in the literature (e.g., Huang and Huang, 2012). In

[21] This assumption is meant to ensure that the amount of debt is comparable across the finite and perpetual debt model versions.

addition, the levered equity risk premium rises to 3.91%, up from 3.18% with perpetual debt.

3.1.4 Predictions

We now explore how the transmission in default risk across borrowers varies with the level of refinancing risk. He and Xiong (2012) find that shorter average debt maturity increases a firm's refinancing risk when secondary debt markets are illiquid, thereby influencing its optimal default policy. While our model abstracts from such liquidity considerations, we expect the refinancing channel to play an important role in driving the response of a borrower's default decision to shocks affecting another borrower and, hence, their co-movement in default risk.

First, we provide intuition regarding how a borrower's debt maturity impacts its optimal default boundary and, as a result, shapes the default risk transmission mechanism uncovered in this paper.

Recall that when a bond matures, it is replaced by a new bond with the same coupon and principal. However, the market price of the new bond may deviate from the principal of the maturing bond. As the bond yield increases (through higher default risk or risk premium), rollover losses arise from issuing new bonds to replace maturing bonds. To avoid default, equity holders may be willing to bear the rollover losses and bail out maturing bond holders to the extent that the equity value remains positive, i.e., the option value of keeping the borrower alive justifies covering the expected rollover losses. With shorter debt maturity, the increase in rollover risk exerts greater pressure on the equity holders to inject funds and makes them less patient, which translates into a higher optimal default boundary, as illustrated in Panel C of Figure 3. The consequence is thus an increase in the *level* of default risk.

This rollover channel generates another central prediction of the model: with shorter debt maturity, a borrower's endogenous default decision becomes more *sensitive* to shocks hitting another borrower. To understand this prediction, consider, as before, a negative shock to tree B, while keeping the output of tree A unchanged. The higher risk premium for tree A increases the cost of replacing each dollar of maturing debt: It increases the pressure on shareholders to bail out existing bondholders and makes the former less patient, thus increasing the default boundary further as the share of tree A rises. Shorter debt maturity exacerbates this effect and will alter the trade-off between defaulting and keeping the borrower alive by injecting funds in favour of defaulting. Panel C of Figure 3 shows that the optimal default boundary and the distance-to-default are thus more sensitive to a change in the

share of tree A (i.e., shocks to tree B) for borrowers with shorter debt maturity.

As a result, the degree of rollover risk, dictated by the maturity structure, directly regulates a borrower's default decision following shocks to other borrowers: the endogenous change in default risk becomes particularly severe for borrowers with shorter-term debt. Consequently, we observe a strengthening in the co-movement in default risk for borrowers with greater rollover risk.

More formally, we can compute the sensitivity of the default boundary to changes in the output share, given in (13), and subsequently the distance-to-default correlation, given in (12). Table 2 presents the correlation between the distance-to-defaults of tree A and tree B for a range of debt maturities. For an average maturity of 10 years ($m_i = 0.1$), we find that $f_A(0.5) = -f_B(0.5) \approx 0.0700$, which yields $\rho_{DD}(0.5) \approx 13.93\%$, compared to 9.51% stated earlier for the perpetual debt case. The correlation further increases to 15.32% for a 5-year average debt maturity.

Confirming these results, Figure 9 shows that the term structure of the default risk correlation is monotonically downward sloping. Notably, we find that the slope is more pronounced for low maturities; this means that changing a debt's maturity from 10 to 5 years increases default risk co-movement more than a change from 10 to 15 years reduces it.

FIGURE 9 ABOUT HERE

Rollover risk also has a meaningful effect on credit spreads. Panel C of Figure 5 shows that the credit spread of tree A is much more sensitive to shocks affecting tree B when rollover risk is higher, that is in the case of shorter debt maturity.

In sum, we find that a shock to one borrower generates a greater impact on the creditworthiness of another borrower if the latter has higher rollover risk, i.e., the risk arising from shorter maturity debt and more frequent debt refinancing. The model thus predicts a stronger level of co-movement in default risk and credit spread as average debt maturity decreases.

3.2 Correlated trees

Our baseline model features independent output streams, given our objective to study a new mechanism for default risk transmission that arises through market clearing rather than through correlated

fundamentals. In many practical situations, such an assumption would not be realistic. In this section, we revisit our model findings when the fundamentals of the two trees are subject to correlated shocks.

Table 4 reports how the total correlation across the trees' distance-to-default (ρ_{DD}) varies with the correlation across fundamentals (ρ), ranging between -0.25 and 0.25. We also report the excess correlation, defined as the correlation in distances-to-default minus the correlation in output shocks, i.e., $\rho_{DD} - \rho$. Overall, the consideration of a non-zero correlation in output shocks does not change our main results qualitatively. The economy continues to feature excess default risk co-movement across borrowers, whether the correlation between trees is positive or negative. In addition, the term structure of the excess default risk correlation remains downward sloping in all cases (see Figure 9).

TABLE 4 ABOUT HERE

Observe, however, that the excess co-movement in default risk strengthens as the correlation between trees becomes weaker. The excess correlation in distances-to-default increases from 7.31% when the correlation in output shocks is 0.25 to 10.46% when the correlation is -0.25. This result arises because a higher output correlation reduces the variability of the output share, and thus the importance of the risk premium channel, which is the key mechanism in our paper. The central takeaway from this analysis is that, while co-movement in default risk naturally increases across borrowers with more correlated fundamentals, the spillover effects we identify act as a substitute to such fundamental correlation. The excess level of co-movement indeed strengthens when both output streams become less exposed to a common source of shocks.

4 Applications

The theory we present in this paper demonstrates how an economy comprising borrowers with independent fundamentals can exhibit co-movement in default risk. The default risk linkages we emphasize, arising from the transmission of risk premia, have broad implications for various areas of financial economics, such as corporate and sovereign debt markets. In the following sections, we delve into several practical applications derived from the predictions of our model.

4.1 Corporate sector

The U.S. economy has experienced significant clusters of corporate defaults over the past century, prompting research efforts to understand the underlying sources of such co-movement in default risk. This is all the more relevant in a world with expanding markets for securities exposed to correlated default risk, such as collateralized debt obligations.

One prominent candidate for the source of default clustering is the joint exposure of firms to common factors such as economic growth, aggregate uncertainty, and monetary policies. While these factors can potentially lead to correlated changes in firms' default rates, the literature suggests that this channel alone cannot fully account for the extent of corporate default clustering observed in the U.S. (e.g., Das et al., 2007). Azizpour et al. (2018) further demonstrate that contagion serves as a significant source of default clustering, even after controlling for firms' joint exposure to observable and latent systematic factors. This finding aligns with a substantial body of literature exploring default risk contagion in the corporate sector.[22]

Our paper contributes to the literature by offering a rationale for the observed co-movement in default risk among firms that do not share strong ties in terms of their fundamentals, business relations, or systematic risk exposure. In addition, we propose a transmission channel that induces co-movement in default risk between firms, even in the absence of financial-network linkages (Allen and Gale, 2000), self-fulfilling beliefs (Goldstein and Pauzner, 2004), or competition across firms (Chen et al., 2023). The transmission channel we propose is distinct from traditional notions of default contagion, as there is no direct causal link between the default events of two borrowers. Instead, our channel operates by facilitating the transmission of shocks from one borrower to the endogenous default decision of other borrowers. This mechanism highlights a new dimension of default risk co-movement that goes beyond traditional explanations.

[22]For example, Lang and Stulz (1992) and Jorion and Zhang (2007) empirically document spillovers from bankruptcies to intra-industry equity prices and default swap spreads, while Jorion and Zhang (2009) find that defaults can have spillover effects on business partners. The default by one firm may also have a direct impact on the conditional default rate of other firms, as in the network models of Acemoglu et al. (2015) or Elliott et al. (2014). Chen et al. (2023) show that competition is a source of credit contagion, as firms compete more aggressively when they are in financial distress. In addition, Kodres and Pritsker (2002) propose an information-based mechanism for contagion to explain contagion across financial markets, while Bae, Karolyi, and Stulz (2003) study credit risk contagion across international markets.

4.2 Bailouts and bankruptcy cascades

During times of crisis, governments often provide financial assistance to the corporate sector in an effort to minimize the number of bankruptcies. Notable examples include the government aid extended to the U.S. airline industry following the September 11, 2001 attacks,[23] the bailouts of the banking and automotive industry during the Great Recession,[24] and the unprecedented economic rescue packages implemented worldwide in response to the COVID-19 crisis.

However, a contentious issue arises when determining which firms should receive the most substantial government support. In many cases, bailout funds are directed towards large firms, which may not necessarily be the most vulnerable entities in the economy. Nevertheless, such interventions can be justified within the context of our model if the policymakers' objective is to mitigate the risk of a widespread wave of corporate bankruptcies.

Our theory suggests that reducing default risk for a specific group of firms generates positive spillover effects on the broader corporate sector. When certain firms receive support and their creditworthiness improves, it leads to a favorable repricing of the remaining firms in the economy, resulting in reduced systematic risk for the latter firms. As a result, these firms experience lower funding costs, decreased rollover risk, and lower default probabilities.

This implies that targeted financial support provided to any sector or industry can have beneficial spillover effects throughout the economy. By reducing default risk for some firms, the support naturally transmits to others, improving the stability and resilience of the corporate sector as a whole. The default linkages predicted by our theory provide insights into how corporate bailouts can mitigate the likelihood of bankruptcy cascades, particularly during economic crises.

4.3 Sovereign debt markets

Default linkages also play a significant role in sovereign debt markets, particularly during periods of sovereign debt crises characterized by waves of defaults. This was evident during the European sovereign debt crisis when the fear of contagion was frequently mentioned in the financial press as a

[23] Congress passed The Air Transportation Safety and System Stabilization Act, which created the office of the Air Transportation Stabilization Board in the Department of the Treasury. They were able to issue $10 billion in loan guarantees to help the airlines in the aftermath.

[24] With bankruptcy looming for General Motors and Chrysler by 2009, the governments of both the United States and Canada intervened, supplying $85 billion that enabled the two companies to restructure their debt.

primary driver of sovereign credit spreads. The concern was that a higher probability of default for one sovereign, such as Greece, could lead to spillover effects, elevating default risk and borrowing costs for other sovereigns like Italy or Spain. European policymakers frequently cited this contagion effect to justify sovereign bailouts and interventions.

A growing theoretical literature has emerged to forward our understanding of the contagion across sovereigns, which has gained significant attention among economists and investors alike. One line of research explores the links between financial networks and default spillovers to model contagion for European sovereigns (e.g., Elliott et al., 2014). However, the impact of financial interconnectedness on sovereign borrowing costs does not appear to be economically significant, as highlighted by Glover and Richards-Shubik (2021). Benzoni, Collin-Dufresne, Goldstein, and Helwege (2015) propose an alternative approach by considering an underlying fundamental economic regime that is shared among all Eurozone member states, yet remains unknown to investors. Their findings demonstrate that a combination of Bayesian updating and fragile beliefs results in equilibrium credit spreads that are substantially higher and more correlated compared to a scenario where there is no uncertainty about the state of the economy.

Complementing this literature, our theory provides insights into understanding default risk linkages in the sovereign debt market. Despite the absence of direct financial or economic linkages between sovereigns in our model, we observe substantial co-movement in default probabilities and credit spreads. This mechanism is particularly relevant for understanding the patterns of default linkages among countries with weak economic interdependencies.

For instance, during the European debt crisis from 2010 to 2012, the initial shock originating in Greece, characterized by a sharp decline in GDP and a surge in debt levels, rapidly spread to other countries. Gabaix and Koijen (2022) extensively documented these spillover effects. As predicted by our model, the contagion effects were most pronounced in countries with high levels of indebtedness and a significant proportion of short-term government debt to refinance. The co-movement in borrowing costs, combined with heightened rollover risk, likely played a pivotal role in transmitting default risk among southern European countries and Ireland.

Our theory can also be useful to understand how a sovereign default crisis can propagate across the world to emerging countries that are fundamentally unrelated. An illustrative case is the events

leading to the Russian sovereign default on August 18, 1998, which had repercussions reaching Brazil and other Latin American countries, despite their limited commercial ties with Russia. For example, Brazil's exports to Russian markets accounted for merely 0.2% of its total exports at that time. Moreover, the correlation in GDP growth rates between Brazil and Russia over the 1990-1998 period, based on World Bank data, was approximately -0.14, indicating that the two economies had largely independent fundamentals. However, Brazil's bond spreads experienced a substantial increase in the months leading up to the Russian crisis. From 387 basis points in April, the spreads rose to 546 basis points in July and further spiked to 1182 basis points in September 1998. Interpreted through our model, the negative real GDP shocks suffered by Russia contributed to heightened risk premia and credit spreads in Brazil even before the actual default event. The subsequent downgrade of Brazilian debt by Moody's in September 1999 underscores the impact of increased refinancing costs on Brazil's default probability.

Overall, our theory can contribute to a better understanding of credit risk spillovers in the sovereign debt market. The central channel for the default risk transmission is the rise in risk premia, which leads to higher borrowing costs for other countries. This framework allows us to explain how adverse economic shocks in one country can affect default risk and credit spreads for other countries, even in the absence of strong fundamental links. While there are likely other mechanisms at play in the transmission of default risk, we are proposing a new, theoretically-motivated channel that appears to be consistent with what we observe empirically.

Understanding the source of default linkages in sovereign debt markets is critical for policymakers. It enables them to develop effective strategies to address the systemic risks associated with sovereign debt crises. By intervening and providing support to distressed sovereigns, policymakers can contain the spread of defaults and mitigate potential contagion effects, thereby promoting stability and resilience in the global financial system.

5 Conclusion

In this paper, we propose an equilibrium asset pricing model with two independent borrowers and uncover a new form of default risk linkages. Specifically, we show that a negative output shock to one borrower not only reduces its own creditworthiness, but also induces the other borrower to become a

larger player in the economy and to bear more systematic risk. The increased risk premium tilts its endogenous default decision towards a more rapid default.

A positive (excess) correlation in default risk across borrowers then emerges, together with co-movement in credit spreads, risk premia, and equity volatility, even when their fundamentals remain independent. We also demonstrate that the transmission in default risk across borrowers is modulated by their refinancing needs. A borrower with more short-term debt bears greater rollover risk and becomes more exposed to this form of spillover.

The default risk linkages we highlight in this paper have broad implications. We explore various applications of our framework, such as corporate borrowing and default clusters, the structuring of corporate sector bailouts during crises, and the observed contagion in the sovereign debt market, particularly in emerging and European countries.

Our theoretical analysis also allows interesting extensions. For instance, the model could be enriched by incorporating a larger number of borrowers. This extension would be particularly relevant in a scenario where the initial distribution of output shares is uneven, as seen in a market where a dominant borrower influences several smaller ones. This concept aligns with the notion of a granular economy (Gabaix, 2011). Notably, this situation holds particular relevance in the current context, where a handful of mega-tech stocks dominate the US equity market. We leave such analysis for future research.

References

Abramowitz, M. and I. A. Stegun (Eds.) (1972). *Handbook of Mathematical Functions*. Dover.

Acemoglu, D., A. Ozdaglar, and A. Tahbaz-Salehi (2015). Systemic risk and stability in financial networks. *American Economic Review 105*(2), 564–608.

Allen, F. and D. Gale (2000). Financial contagion. *Journal of Political Economy 108*(1), 1–33.

Azizpour, S., K. Giesecke, and G. Schwenkler (2018). Exploring the sources of default clustering. *Journal of Financial Economics 129*(1), 154–183.

Bae, K.-H., G. A. Karolyi, and R. M. Stulz (2003). A new approach to measuring financial contagion. *Review of Financial Studies 16*(3), 717–763.

Bai, J., R. S. Goldstein, and F. Yang (2020). Is the credit spread puzzle a myth? *Journal of Financial Economics 137*(2), 297–319.

Bao, J., K. Hou, and S. Zhang (2023). Systematic default and return predictability in the stock and bond markets. *Journal of Financial Economics, Forthcoming*.

Bekaert, G., M. Ehrmann, M. Fratzscher, and A. Mehl (2014). The global crisis and equity market contagion. *The Journal of Finance 69*(6), 2597–2649.

Benzoni, L., P. Collin-Dufresne, R. S. Goldstein, and J. Helwege (2015). Modeling credit contagion via the updating of fragile beliefs. *The Review of Financial Studies 28*(7), 1960–2008.

Bhamra, H. S., C. Dorion, A. Jeanneret, and M. Weber (2023). High inflation: Low default risk and low equity valuations. *The Review of Financial Studies 36*(3), 1192–1252.

Bhamra, H. S., L.-A. Kuehn, and I. A. Strebulaev (2010). The levered equity risk premium and credit spreads: A unified framework. *The Review of Financial Studies 23*(2), 645–703.

Bharath, S. T. and T. Shumway (2008). Forecasting default with the Merton distance to default model. *The Review of Financial Studies 21*(3), 1339–1369.

Boyer, B. H., T. Kumagai, and K. Yuan (2006). How do crises spread? Evidence from accessible and inaccessible stock indices. *The Journal of Finance 61*(2), 957–1003.

Buraschi, A., F. Trojani, and A. Vedolin (2014). When uncertainty blows in the orchard: Comovement and equilibrium volatility risk premia. *The Journal of Finance 69*(1), 101–137.

Campbell, J. Y., J. Hilscher, and J. Szilagyi (2008). In search of distress risk. *The Journal of Finance 63*(6), 2899–2939.

Chaderina, M., P. Weiss, and J. Zechner. The maturity premium. *Journal of Financial Economics 144*(2), 670–694.

Chang, G. and S. Sundaresan (2005). Asset prices and default-free term structure in an equilibrium model of default. *The Journal of Business 78*(3), 997–1022.

Chen, H. (2010). Macroeconomic conditions and the puzzles of credit spreads and capital structure. *The Journal of Finance 65*(6), 2171–2212.

Chen, H., R. Cui, Z. He, and K. Milbradt (2018). Quantifying liquidity and default risks of corporate bonds over the business cycle. *The Review of Financial Studies 31*(3), 852–897.

Chen, H., W. Dou, H. Guo, and Y. Ji (2023). Feedback and contagion through distressed competition. *Working Paper, MIT*.

Chen, L., P. Collin-Dufresne, and R. S. Goldstein (2008). On the relation between the credit spread puzzle and the equity premium puzzle. *The Review of Financial Studies 22*(9), 3367–3409.

Choi, J., D. Hackbarth, and J. Zechner (2018). Corporate debt maturity profiles. *Journal of Financial Economics 130*(3), 484–502.

Cochrane, J. H., F. A. Longstaff, and P. Santa-Clara (2008). Two trees. *Review of Financial Studies 21*(1), 347–385.

Cryer, C. (1971). The solution of a quadratic programming problem using systematic overrelaxation. *SIAM Journal of Control 9*, 385–392.

Dangl, T. and J. Zechner (2021). Debt maturity and the dynamics of leverage. *The Review of Financial Studies 34*(12), 5796–5840.

Das, S. R., D. Duffie, N. Kapadia, and L. Saita (2007). Common failings: How corporate defaults are correlated. *The Journal of Finance 62*(1), 93–117.

Davydenko, S. A. and I. A. Strebulaev (2007). Strategic actions and credit spreads: An empirical investigation. *The Journal of Finance 62*(6), 2633–2671.

Driessen, J. (2005). Is default event risk priced in corporate bonds? *The Review of Financial Studies 18*(1), 165–195.

Duffie, D., L. Saita, and K. Wang (2007). Multi-period corporate default prediction with stochastic covariates. *Journal of Financial Economics 83*(3), 635–665.

Dumas, B. (1992). Dynamic equilibrium and the real exchange rate in a spatially separated world. *The Review of Financial Studies 5*(2), 153–180.

Elliott, M., B. Golub, and M. O. Jackson (2014). Financial networks and contagion. *American Economic Review 104*(10), 3115–53.

Ericsson, J. and O. Renault (2006). Liquidity and credit risk. *The Journal of Finance 61*(5), 2219–2250.

Fan, H. and S. M. Sundaresan (2000). Debt valuation, renegotiation, and optimal dividend policy. *The Review of Financial Studies 13*(4), 1057–1099.

Feldhütter, P. and S. M. Schaefer (2018). The myth of the credit spread puzzle. *The Review of Financial Studies 31*(8), 2897–2942.

Friewald, N., F. Nagler, and C. Wagner (2022). Debt refinancing and equity returns. *Journal of Finance 77*(4), 2287–2329.

Fudenberg, D. and E. Maskin (1986). The folk theorem in repeated games with discounting or with incomplete information. *Econometrica 54*(3), 533–554.

Gabaix, X. (2011). The granular origins of aggregate fluctuations. *Econometrica 79*(3), 733–772.

Gabaix, X. and R. S. Koijen (2022). Granular instrumental variables. Technical report, National Bureau of Economic Research.

Geske, R. (1977). The valuation of corporate liabilities as compound options. *Journal of Financial Economics 4*(4), 541–552.

Glover, B. and S. Richards-Shubik (2021). Contagion in the European sovereign debt crisis. *Carnegie Mellon University, Working Paper*.

Goldstein, I. and A. Pauzner (2004). Contagion of self-fulfilling financial crises due to diversification of investment portfolios. *Journal of Economic Theory 119*(1), 151–183.

Hamao, Y., R. W. Masulis, and V. Ng (1990). Correlations in price changes and volatility across international stock markets. *Review of Financial Studies 3*(2), 281–307.

Hasler, M. and C. Ornthanalai (2018). Fluctuating attention and financial contagion. *Journal of Monetary Economics 99*, 106–123.

He, Z. and K. Milbradt (2014). Endogenous liquidity and defaultable bonds. *Econometrica 82*(4), 1443–1508.

He, Z. and W. Xiong (2012). Rollover risk and credit risk. *The Journal of Finance 67*(2), 391–430.

Herskovic, B., B. Kelly, H. Lustig, and S. Van Nieuwerburgh (2016). The common factor in idiosyncratic volatility: Quantitative asset pricing implications. *Journal of Financial Economics 119*(2), 249–283.

Herskovic, B., B. T. Kelly, H. N. Lustig, and S. Van Nieuwerburgh (2020). Firm volatility in granular networks. *Journal of Political Economy 128*(11), 4097–4162.

Huang, J.-Z. and M. Huang (2012). How much of the corporate-treasury yield spread is due to credit risk? *The Review of Asset Pricing Studies 2*(2), 153–202.

Jorion, P. and G. Zhang (2007). Good and bad credit contagion: Evidence from credit default swaps. *Journal of Financial Economics 84*(3), 860–883.

Jorion, P. and G. Zhang (2009). Credit contagion from counterparty risk. *The Journal of Finance 64*(5), 2053–2087.

Kang, J. and C. E. Pflueger (2015). Inflation risk in corporate bonds. *The Journal of Finance 70*(1), 115–162.

Kodres, L. E. and M. Pritsker (2002). A rational expectations model of financial contagion. *Journal of Finance 57*(2), 769–799.

Lang, L. H. and R. Stulz (1992). Contagion and competitive intra-industry effects of bankruptcy announcements: An empirical analysis. *Journal of Financial Economics 32*(1), 45–60.

Leland, H. E. (1994). Corporate debt value, bond covenants, and optimal capital structure. *Journal of Finance 49*(4), 1213–52.

Leland, H. E. (1998). Agency costs, risk management, and capital structure. *The Journal of Finance 53*(4), 1213–1243.

Leland, H. E. and K. B. Toft (1996). Optimal capital structure, endogenous bankruptcy, and the term structure of credit spreads. *The Journal of Finance 51*(3), 987–1019.

Martin, I. W. R. (2013). Consumption-based asset pricing with higher cumulants. *Review of Economic Studies 80*(2), 745–773.

Menzly, L., T. Santos, and P. Veronesi (2004). Understanding predictability. *Journal of Political Economy 112*(1), 1–47.

Merton, R. C. (1974). On the pricing of corporate debt: The risk structure of interest rates. *The Journal of Finance 29*(2), 449–470.

Pavlova, A. and R. Rigobon (2007). Asset prices and exchange rates. *The Review of Financial Studies 20*(4), 1139–1180.

Peskir, G. and A. N. Shiryaev (2006). *Optimal Stopping and Free-Boundary Problems*. Lectures in Mathematics, ETH Zürich, Birkhäuser.

Santos, T. and P. Veronesi (2010). Habit formation, the cross section of stock returns and the cash-flow risk puzzle. *Journal of Financial Economics 98*(2), 385–413.

Sauzet, M. (2022). Two investors, two trees, two goods. *Boston University, Working Paper*.

Smith, G. D. (1985). *Numerical solution of partial differential equations: Finite difference methods, Third Edition*. Oxford university press.

Standard and Poor's (2021). Default, transition, and recovery: 2020 annual global corporate default and rating transition study. *New York: S&P Global*.

Table 1. Model calibration

This table reports parameter values in the model calibration. Bold figures correspond to the baseline case. Values are annualized when applicable.

Parameter	**Notation**	**Values**
Output growth (tree A)	μ_A	0.02
Output growth (tree B)	μ_B	0.02
Output growth volatility (tree A)	σ_A	0.20
Output growth volatility (tree B)	σ_B	0.20
Correlation between output shocks	ρ	[-0.25, **0**, 0.25]
Debt coupon (tree A)	C_A	[0.2, **0.4**, 0.6]
Debt coupon (tree B)	C_B	0.4
Bond maturity	$1/m$	[5, 10, 30, ∞]
Bankruptcy cost	ϵ	0.622
Tax rate	φ	0.15
Preference for time	δ	0.06

Table 2. Default risk correlation and rollover risk

This table presents the correlation between the distances-to-default of trees A and B (given by ρ_{DD}) in different economic environments. Each row reports the predictions for a given average debt maturity (equal to $1/m$), where lower debt maturity translates into higher rollover risk. Each column considers a different output share of tree A (measured by s), where variation in the output share is obtained by changing the output level of tree B, keeping the output level of tree A constant. The output shocks are independent across trees ($\rho = 0$). Each panel presents predictions for different liquidation outcomes in default. In Panel A, the baseline case, shareholders recover nothing in default and the full liquidation costs are paid by the debtholders. In Panel B, shareholders and debtholders recover half of the liquidation costs, following a Nash bargaining game (Fan and Sundaresan, 2000). Sections 2.1 and 3.1.3 discuss the model calibration.

	Share of tree A (s)				
	20%	35%	50%	65%	80%
Panel A: baseline model					
Debt maturity ($1/m$)					
Perpetual	9.89%	9.65%	9.51%	9.65%	9.89%
30 year	12.40%	11.95%	11.80%	11.95%	12.40%
10 year	14.48%	14.00%	13.93%	14.00%	14.48%
5 year	15.77%	15.41%	15.32%	15.41%	15.77%
Panel B: with renegotiation in default					
Debt maturity ($1/m$)					
Perpetual	9.91%	9.64%	9.55%	9.64%	9.91%
30 year	11.90%	11.33%	11.17%	11.33%	11.90%
10 year	13.77%	12.95%	12.75%	12.95%	13.77%
5 year	14.86%	14.05%	13.78%	14.05%	14.86%

Table 3. Default risk co-movement in simulated economies

This table presents results on the co-movement in default risk and asset pricing moments across trees based on a large cross-section of simulated economies. We simulate 20,000 two-tree economies at the daily frequency over a 10-year period using the parameters of the baseline calibration in Table 1. Panel A reports the default probability computed at the 1-, 5-, and 10-year horizons. The empirical counterparts are the cumulative default rates for all-rated corporate bonds in the U.S. from Standard and Poor's (2021). Panel B reports the unconditional default risk correlation across trees, averaged across simulations. Panel C reports the unconditional correlation in key asset pricing moments across trees, also averaged across simulations. Additional statistics include the median and the 5th/95th percentile of all simulations. Section 2.1 discusses the model calibration, while Appendix G provides details on the simulation procedure.

	Baseline model		**Empirical data**	
Panel A: default probabilities				
1-year default rate	1.41%		1,86%	
5-year default rate	6.29%		7.72%	
10-year default rate	11.79%		11.37%	
	Mean	**Median**	**5th**	**95th**
Panel B: default risk correlations across trees				
Distance-to-default	10.06%	10.05%	6.09%	14.01%
10-year default probability	10.84%	10.88%	4.55%	16.88%
Leverage	14.84%	15.00%	10.30%	18.94%
Credit spread	28.08%	28.97%	12.79%	41.02%
Panel C: correlations in asset pricing moments across trees				
Equity volatility	23.75%	21.93%	3.15%	52.06%
Equity risk premium	37.60%	40.23%	−37.87%	86.45%
Debt volatility	45.47%	43.56%	6.19%	89.48%
Debt risk premium	68.22%	78.18%	18.36%	95,79%

Table 4. Default risk correlation with correlated trees

This table presents the main output of the model for distinct levels of correlation across output shocks (given by ρ). Each panel reports the distance-to-default (DD) of both trees, the correlation between their DD (ρ_{DD}), and the corresponding excess correlation ($\rho_{DD} - \rho$). Each column considers a different output share of tree A (measured by s), where variation in the output share is obtained by changing the output level of tree B, keeping the output level of tree A constant. Section 2.1 discusses the model calibration.

	Share of tree A (s)				
	20%	35%	50%	65%	80%
Panel A: independent trees ($\rho = 0$)					
Distance-to-default (DD) of tree A	7.62	7.35	7.17	7.05	6.96
Distance-to-default (DD) of tree B	13.89	10.15	7.17	4.25	0.69
DD correlation (ρ_{DD})	9.89%	9.65%	9.51%	9.65%	9.89%
Excess DD correlation ($\rho_{DD} - \rho$)	9.89%	9.65%	9.51%	9.65%	9.89%
Panel B: negatively correlated trees ($\rho = -0.25$)					
Distance-to-default (DD) of tree A	7.74	7.41	7.23	7.08	6.96
Distance-to-default (DD) of tree B	13.90	10.18	7.23	4.31	0.81
DD correlation (ρ_{DD})	−13.76%	−14.44%	−14.54%	−14.44%	−13.76%
Excess DD correlation ($\rho_{DD} - \rho$)	11.24%	10.56%	10.46%	10.56%	11.24%
Panel C: positively correlated trees ($\rho = 0.25$)					
Distance-to-default (DD) of tree A	7.50	7.26	7.11	7.02	6.93
Distance-to-default (DD) of tree B	13.86	10.12	7.11	4.16	0.57
DD correlation (ρ_{DD})	32.28%	32.31%	32.31%	32.31%	32.28%
Excess DD correlation ($\rho_{DD} - \rho$)	7.28%	7.31%	7.31%	7.31%	7.28%

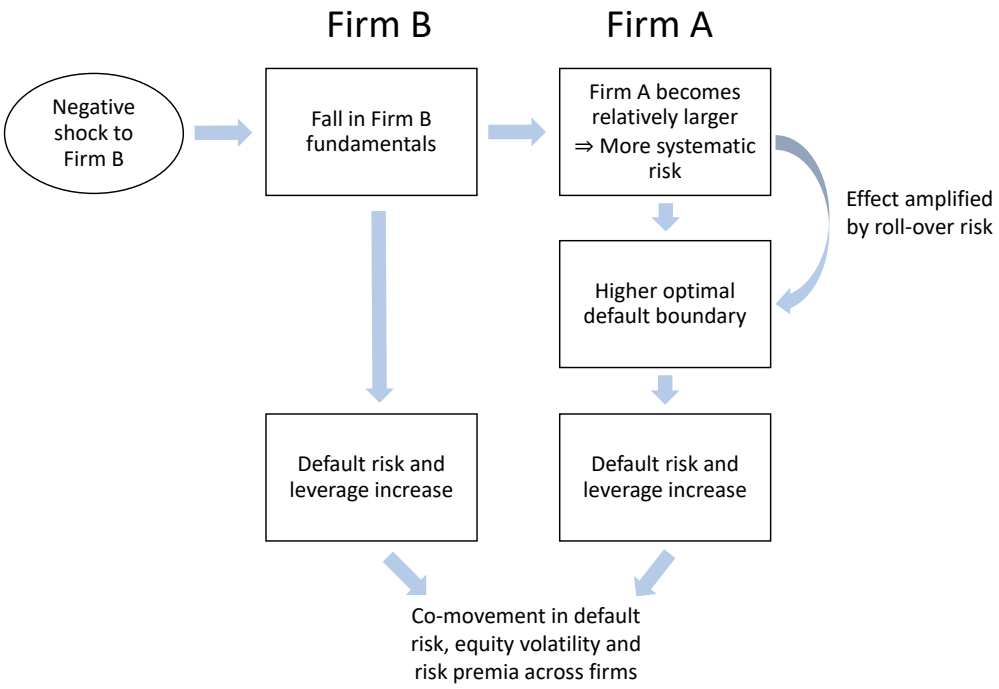

Figure 1. The default risk co-movement mechanism

This figure summarizes the mechanism through which negative shocks to one firm can increase the default risk, equity volatility and risk premium of other firms, even those that are fundamentally unrelated.

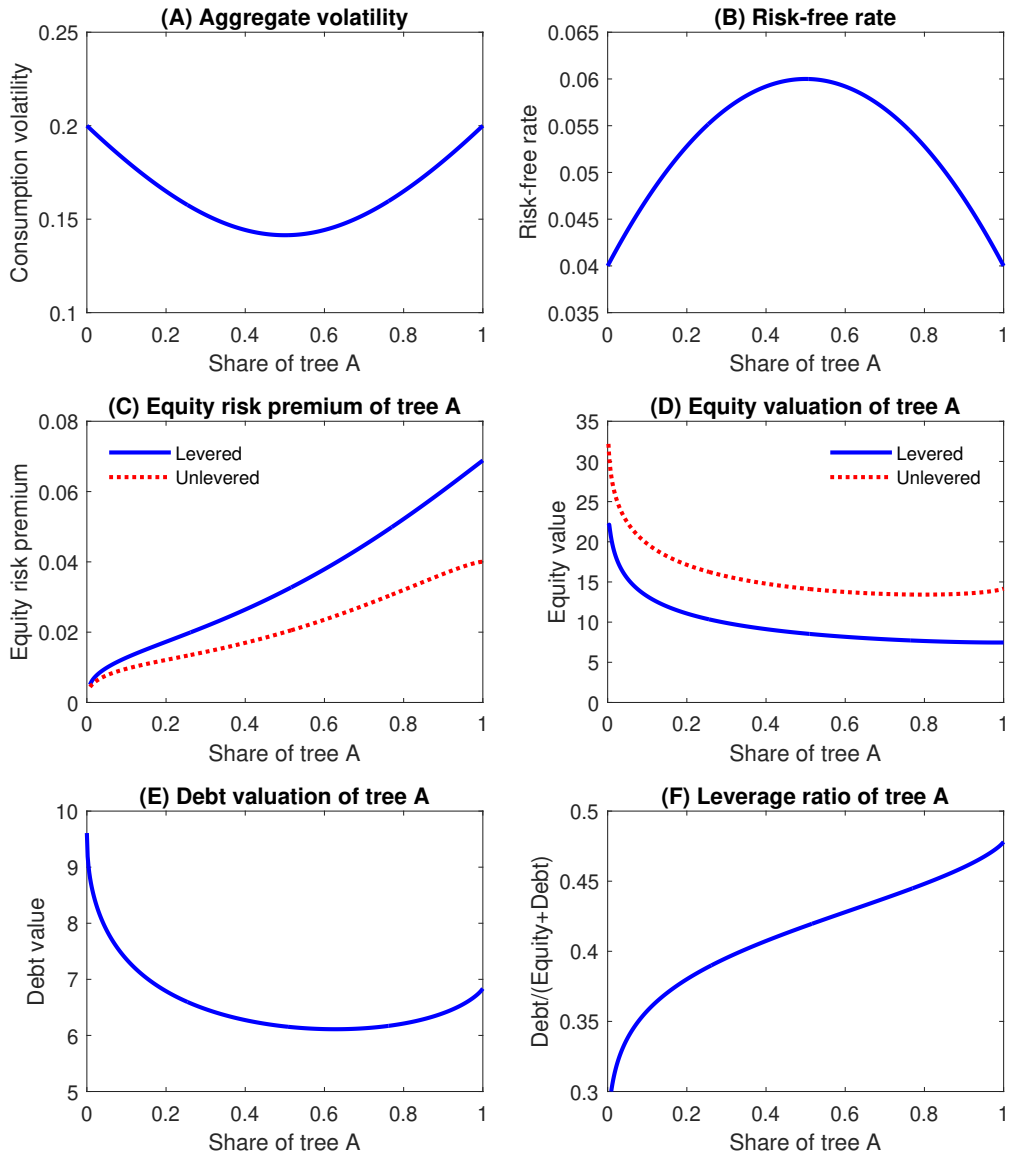

Figure 2. Equilibrium asset pricing quantities

This figure presents the equilibrium asset pricing quantities of our model with two levered trees. Panel A reports the level of aggregate consumption volatility, while Panel B reports the equilibrium risk-free rate. Panels C and D present the equity risk premium and equity value of tree A, for the unlevered and levered cases. Panel E reports the debt value of tree A. Panel F reports the leverage ratio of tree A, which is defined as the value of debt over the value of equity plus debt. Predictions are plotted against the output share of tree A (measured by s), where variation in the output share is obtained by changing the output level of tree B, keeping the output level of tree A constant. Section 2.1 discusses the model calibration. Values are annualized where applicable.

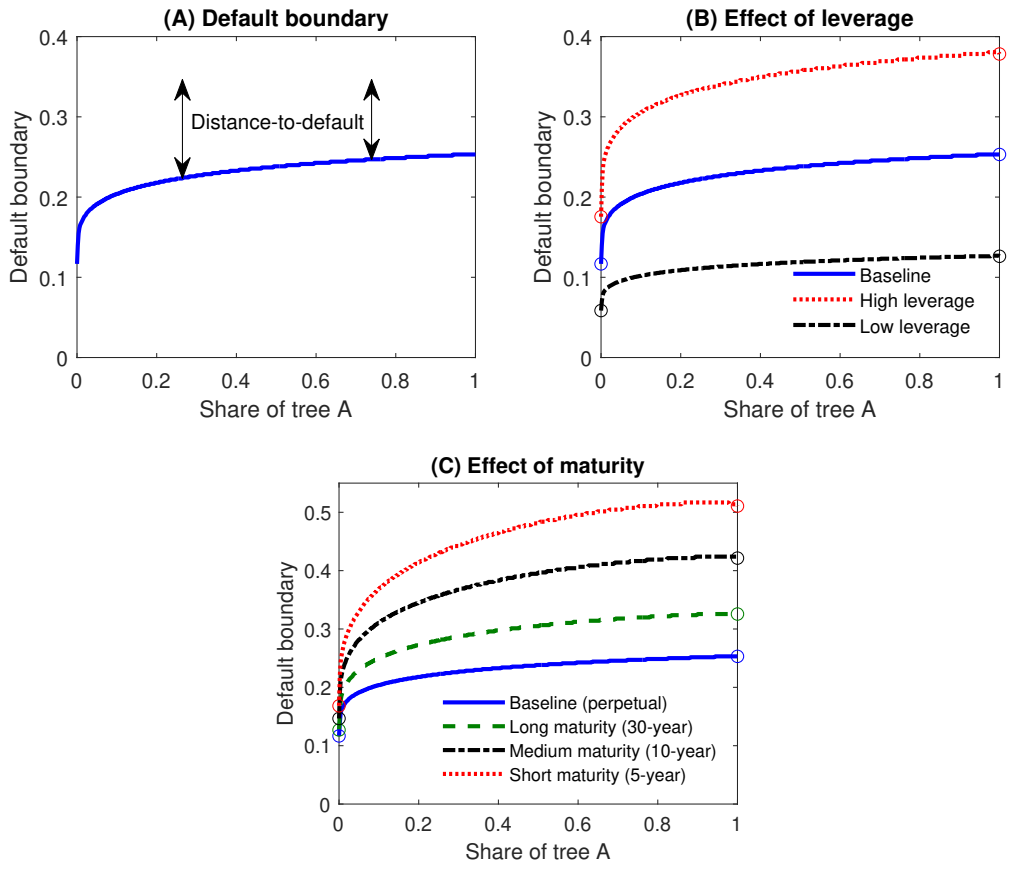

Figure 3. Optimal default policy in a two-tree economy

This figure presents a borrower's optimal default policy in a model with two levered trees. Panel A shows the conditional default boundary of tree A, where a higher value means higher default risk (or lower distance-to-default). In Panel B, each curve presents the endogenous default boundary of tree A for a different level of debt coupon, generating different leverage ratios. In Panel C, each curve presents the endogenous default boundary of tree A for a different average debt maturity, capturing different degrees of rollover risk. The default boundaries are expressed as a fraction of the initial output level. The predictions are plotted against the output share of tree A (measured by s), where variation in the output share is obtained by changing the output level of tree B, keeping the output level of tree A constant. Sections 2.1 and 3.1.3 discuss the model calibration.

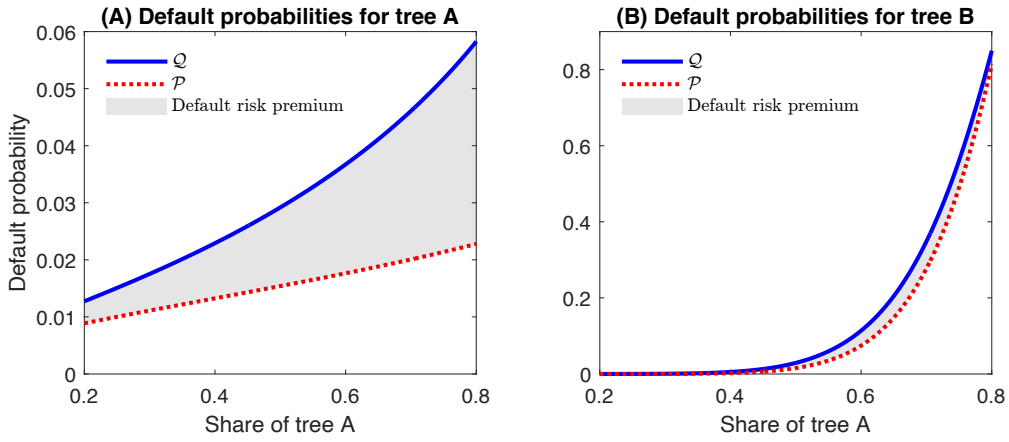

Figure 4. Co-movement in default probabilities

This figure illustrates the co-movement in physical and risk-neutral default probabilities across independent borrowers. The difference between the two measures of default probability identifies the risk premium associated with default risk. The predictions are plotted against the output share of tree A (measured by s), where variation in the output share is obtained by changing the output level of tree B, keeping the output level of tree A constant. Section 2.1 discusses the model calibration.

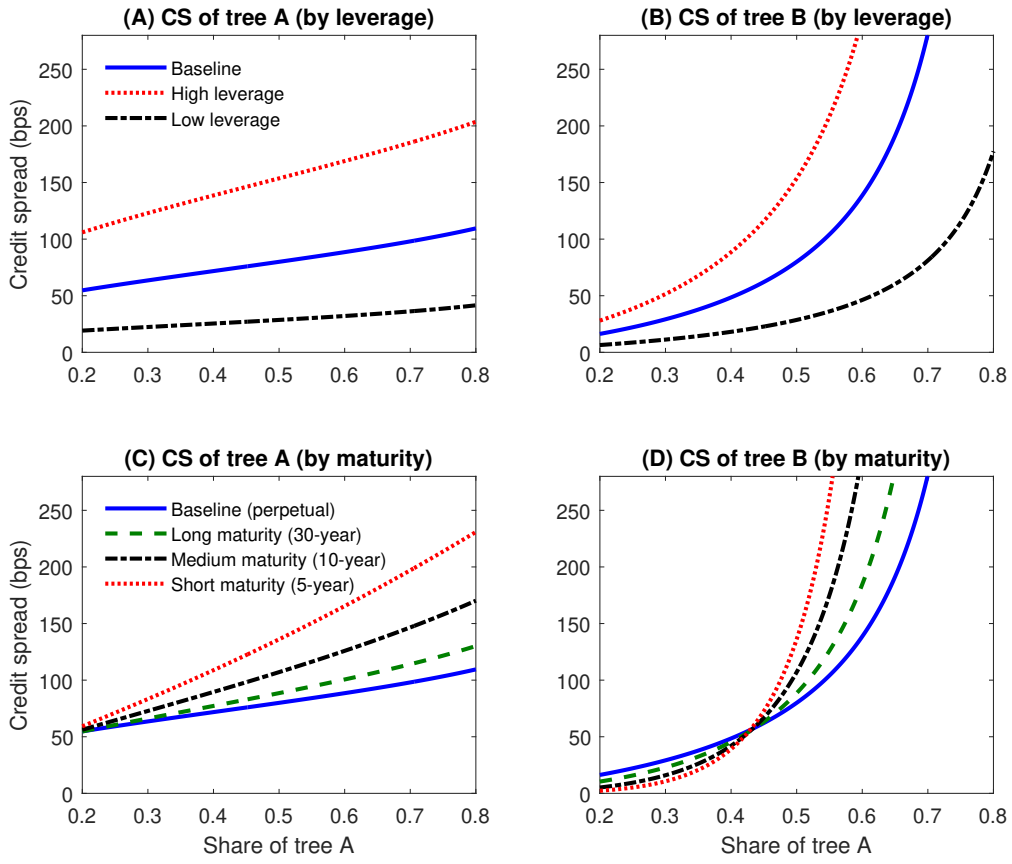

Figure 5. Co-movement in credit spreads

This figure illustrates the co-movement in credit spreads (CS) across independent borrowers. Panel A (B) presents the predictions for tree A (B) for different levels of debt coupon, generating different leverage ratios. Panel C (D) presents the predictions for tree A (B) for various average debt maturities, capturing different degrees of rollover risk. The predictions are plotted against the output share of tree A (measured by s), where variation in the output share is obtained by changing the output level of tree B, keeping the output level of tree A constant. Sections 2.1 and 3.1.3 discuss the model calibration.

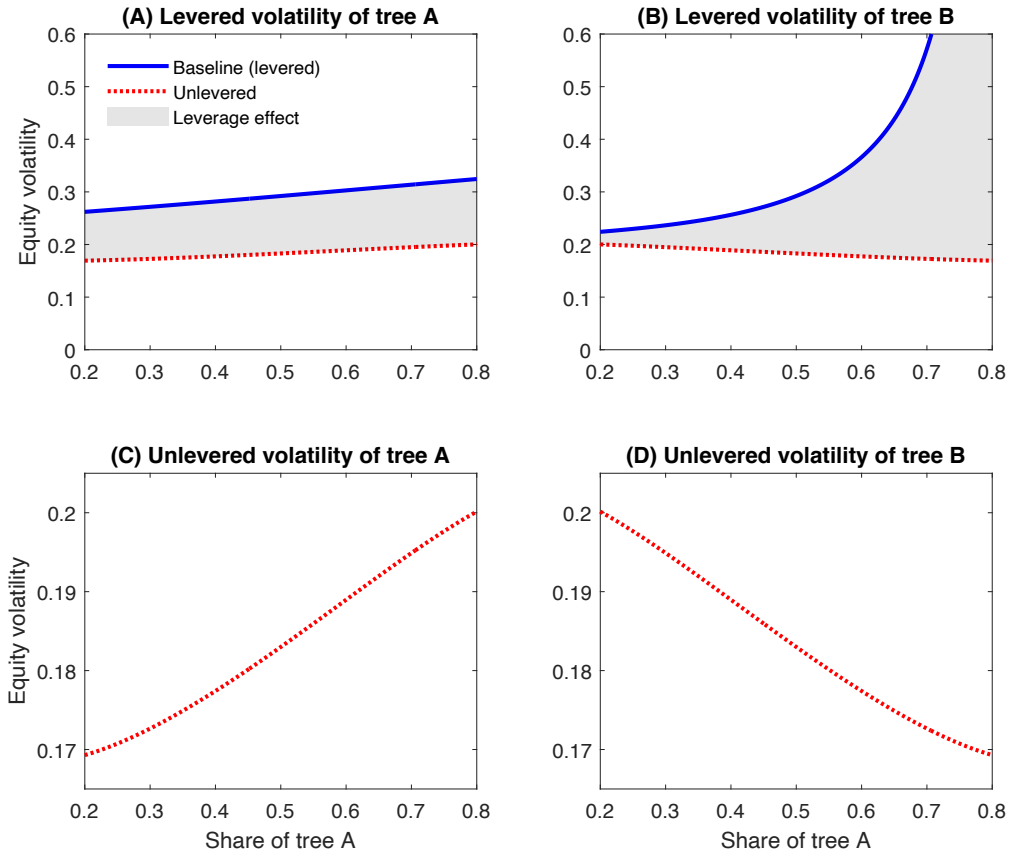

Figure 6. Co-movement in equity volatility

This figure illustrates the co-movement in equity volatility across independent borrowers. Panels A and B present the levered equity volatility of tree A and B, respectively. Panels C and D reproduce Panels A and B in the case of unlevered trees, which corresponds to the case of Cochrane et al. (2008). The predictions are plotted against the output share of tree A (measured by s), where variation in the output share is obtained by changing the output level of tree B, keeping the output level of tree A constant. Section 2.1 discusses the model calibration.

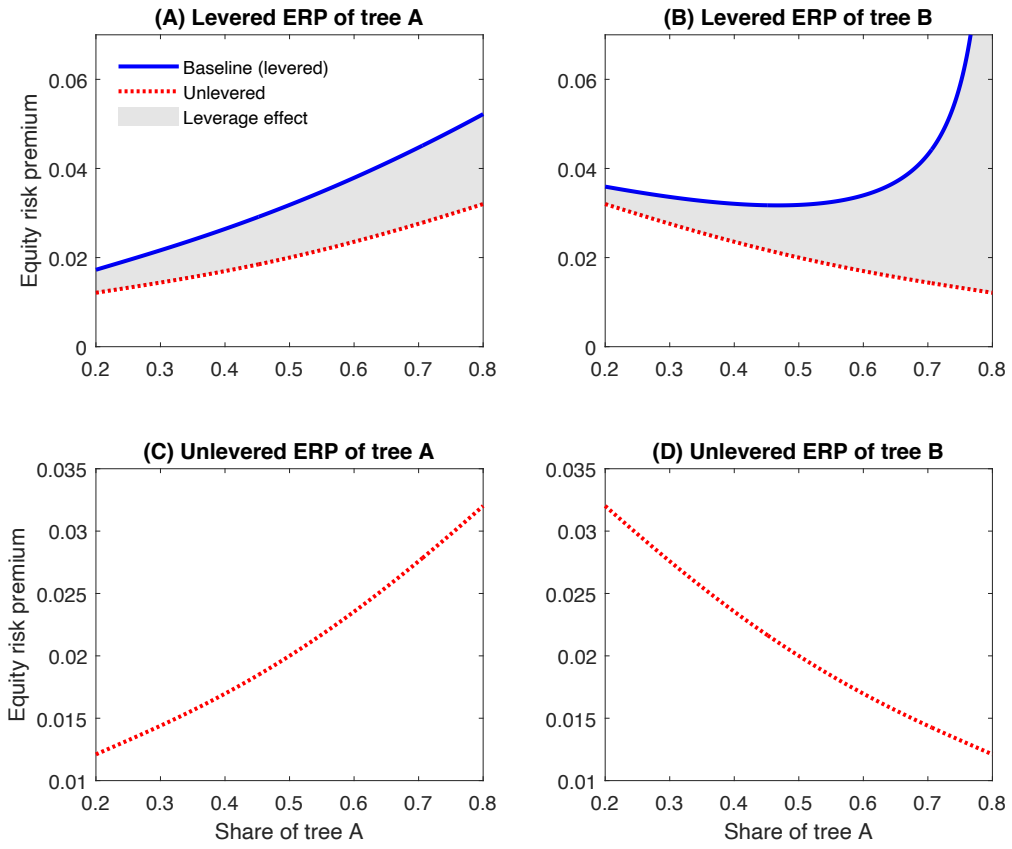

Figure 7. Co-movement in equity risk premium

This figure illustrates the co-movement in equity risk premium (ERP) across independent borrowers. Panels A and B present the levered equity risk premium of tree A and B, respectively. Panels C and D reproduce Panels A and B in the case of unlevered trees, which corresponds to the case of Cochrane et al. (2008). The predictions are plotted against the output share of tree A (measured by s), where variation in the output share is obtained by changing the output level of tree B, keeping the output level of tree A constant. Section 2.1 discusses the model calibration.

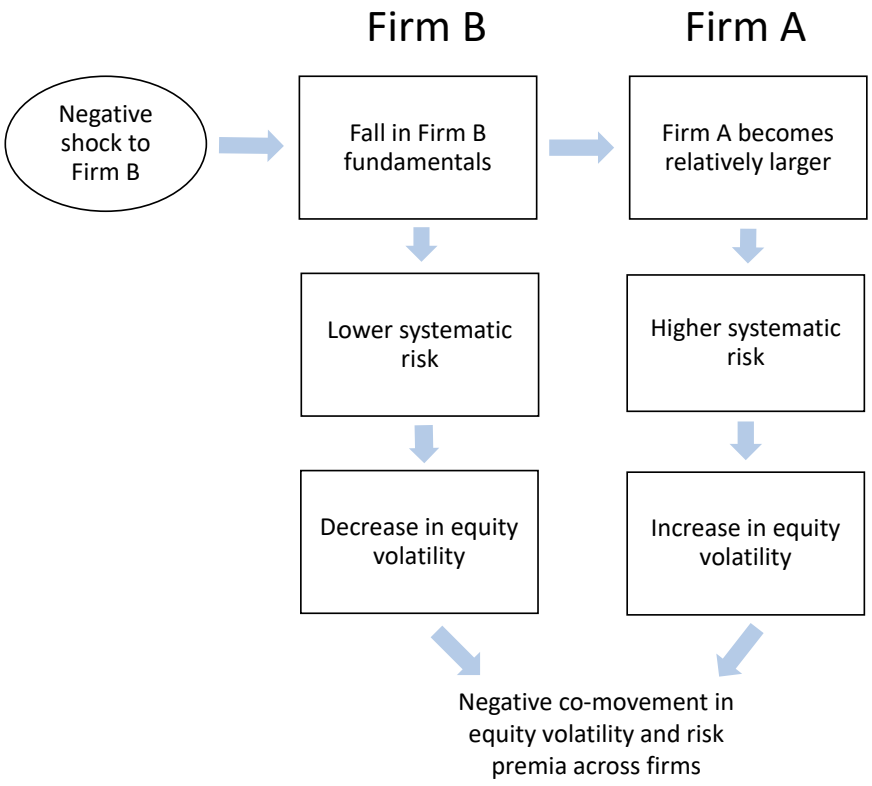

Figure 8. Co-movement in equity volatility and risk premia across unlevered trees

This figure summarizes the mechanism driving the negative co-movement in equity volatility and risk premia across unlevered trees, as in Cochrane et al. (2008). The case of levered trees is illustrated in Figure 1.

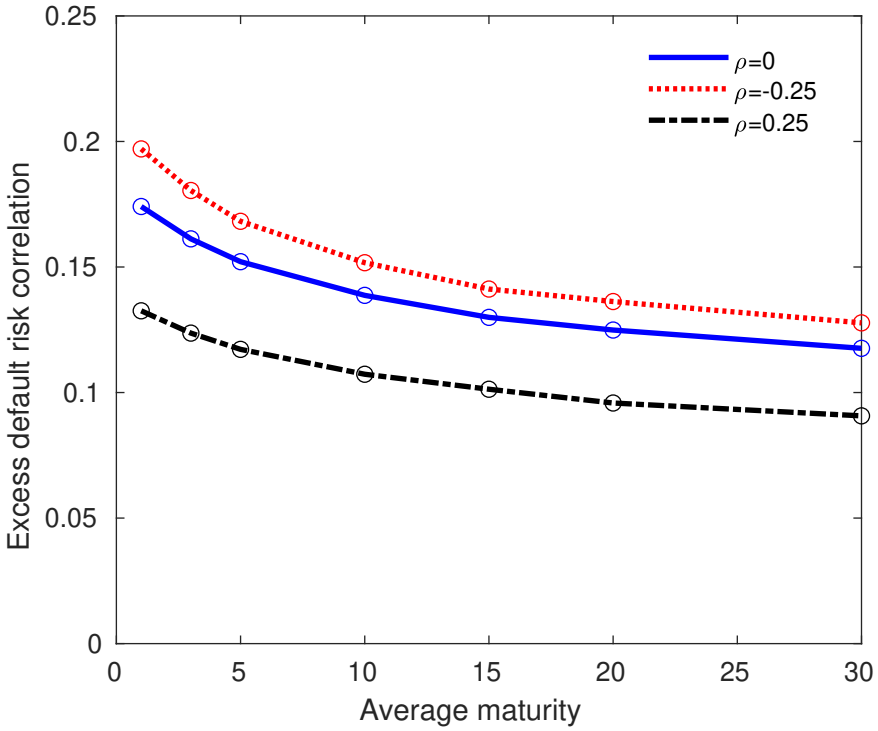

Figure 9. The term structure of excess default risk correlations

This figure illustrates the term structure of the excess default risk correlation, computed as the correlation between each tree's distance-to-default (ρ_{DD}) minus the correlation between their output shocks (ρ). We consider different levels of average debt maturity, between 1 and 30 years, given by $(1/m_i)$. The predictions are plotted for different levels of output correlation (ρ), at the output share $s_t = 0.5$. Sections 2.1 and 3.1.3 discuss the model calibration.

Internet Appendix to

Default Risk Linkages in a Structural Credit Model

(Not for publication)

This Internet Appendix presents supplementary material and results not included in the main body of the paper.

A Numerical procedure for the baseline model

This appendix provides details on the numerical solution of the borrowers' equity valuation in (8) and the debt valuation in (10). The borrowers' endogenous default decision and the two-dimensional stochastic discount factor imply that (8) is a fully two-dimensional optimal stopping problem. We first solve this optimal stopping problem via the numerical solution of an associated free-boundary problem, whose solution provides both the equity value as a function of X_t^i and s_t, and the default boundary as a function of s_t. Once the borrower's optimal default strategy is determined, the debt value in (10) can be solved numerically via an associated *fixed*-boundary problem, providing the debt value as a function of X_t^i and s_t.

Before turning to the levered problem, recall that the value of the unlevered tree is given by (9), i.e. $U^i(s_t) = (1-\varphi)X_t^i V^i(s_t)$, where $V^i(s)$ has the following closed-form solution (Cochrane et al., 2008):

$$V^i(s) = \frac{F\left(1, 1-\gamma, 2-\gamma; \frac{s}{s-1}\right)}{\psi(1-\gamma)(1-s)} + \frac{F\left(1, \theta, 1+\theta; \frac{s-1}{s}\right)}{\psi\theta s} \tag{A.1}$$

with $\gamma = (\nu-\psi)/\eta^2$, $\theta = (\nu+\psi)/\eta^2$, $\psi = \sqrt{\nu^2+2\delta\eta^2}$, $\nu = \mu_B - \mu_A - \sigma_B^2/2 + \sigma_A^2/2$ and $\eta^2 = \sigma_A^2 + \sigma_B^2 - 2\rho\sigma_A\sigma_B$, where F denotes the standard hypergeometric function (see Abramowitz and Stegun, 1972, Chapter 15).

Next, we assume that the optimal default time in (8) is of the form $\tau_i = \inf\{u \geq t \,|\, X_u^i \leq b_i(s_u)\}$, i.e. the first time that the output process X_t drops below some (s_t-dependent) boundary. Setting $X_t^i = x$ and $s_t = s$, standard arguments (e.g., see Peskir and Shiryaev, 2006) reveal that borrower i's optimal stopping problem must also satisfy the following free-boundary problem:

$$\begin{cases} \mathbb{L}_{(X^i,s)}E^i(x,s) - r(s)E^i(x,s) + (1-\varphi)(x-C_i) = 0, & x > b_i(s), \\ E^i(x,s) = 0, & x \leq b_i(s), \\ \frac{\partial E^i}{\partial x}(x,s) = 0 \text{ and } \frac{\partial E^i}{\partial s}(x,s) = 0, & x = b_i(s), \end{cases} \tag{A.2}$$

where $r(s)$ is the risk-free rate defined in (7) and $\mathbb{L}_{(X^i,s)}$ is the infinitesimal generator of the two-

dimensional diffusion (X_t^i, s_t) under the risk-neutral measure, given by

$$\begin{aligned}\mathbb{L}_{(X^i,s)} = &\frac{1}{2}\sigma_i^2 x^2 \frac{\partial^2}{\partial x^2} + \frac{1}{2}\eta^2 s^2 (1-s)^2 \frac{\partial^2}{\partial s^2} + \sigma_i(\sigma_i - \rho\sigma_{-i})(I_A - I_B)xs(1-s)\frac{\partial^2}{\partial x \partial s} \\ &+ \big[\eta^2(I_A - s) + \sigma_i(\sigma_i - \rho\sigma_{-i})(I_B - I_A) + \alpha(s)\big]s(1-s)\frac{\partial}{\partial s} \\ &+ \big[\mu_i - \sigma_i^2 + \sigma_i(\sigma_i - \rho\sigma_{-i})\big(I_A + (I_B - I_A)s\big)\big]x\frac{\partial}{\partial x},\end{aligned} \tag{A.3}$$

where

$$\alpha(s) := \mu_A - \mu_B - s\sigma_A^2 + (1-s)\sigma_B^2 + 2(s - 1/2)\rho\sigma_A\sigma_B \tag{A.4}$$

and I_j denotes the indicator function which is equal to one when $i = j$, and zero otherwise. Note that the two derivatives at $x = b_i(s)$ in (A.2) correspond to the *smooth pasting conditions* which ensure optimality of the boundary $b_i(s)$.

To approximate the solution to (A.2) numerically, we discretize the problem using a second-order finite differencing scheme and then solve the resulting system of equations using the Projected Successive Over Relaxation (PSOR) algorithm. A more detailed description of the PSOR method, along with proofs of convergence, can be found in Cryer (1971). More details about the discretization and implementation of the algorithm can also be made available from the authors upon request.

Once the default boundary $b_i(s)$ has been obtained via (A.2), it can then be used to solve for the value of debt in (10). Similar to the borrowers' equity problem, the value of debt satisfies the following (fixed) boundary value problem:

$$\begin{cases} \mathbb{L}_{(X^i,s)} D^i(x,s) - r(s)D^i(x,s) + C_i = 0, & x > b_i(s), \\ D^i(x,s) = (1-\epsilon)U^i(x,s), & x \leq b_i(s). \end{cases} \tag{A.5}$$

To approximate the solution to (A.5) numerically, we again discretize the problem with the same second-order differencing scheme and solve the resulting system of equations. Since the boundary b_i is known, the standard Successive Over Relaxation (SOR) algorithm suffices.

Finally, in order to obtain accurate results for the numerical solution to (A.2) and (A.5), we define the boundary conditions on both E^i and D^i for $s = 0$ and $s = 1$. For both of these limits, the optimal stopping problem in (8) has a closed-form solution, which we will outline below.

A.1 The limit as $s \to 1$

The limit as $s \to 1$ corresponds to the solution to the problem when tree A dominates the economy and tree B is atomistic. In this limit $E^i(x,s) \to E_1^i(x)$ and the free-boundary problem in (A.2) reduces to

$$\begin{cases} \mathbb{L}^1_{X^i} E_1^i(x) - r^1 E_1^i(x) + (1-\varphi)(x - C_i) = 0, & x > b_i^1, \\ E_1^i(x) = 0, & x \le b_i^1, \\ \frac{dE_1^i}{dx}(x) = 0, & x = b_i^1. \end{cases} \tag{A.6}$$

where $r^1 = r(1) = \delta + \mu_A - \sigma_A^2$ and

$$\mathbb{L}^1_{X^i} = \frac{1}{2}\sigma_i^2 x^2 \frac{\partial^2}{\partial x^2} + (\mu_i - \sigma_i^2 + \sigma_i(\sigma_i - \rho\sigma_{-i})I_B)x\frac{\partial}{\partial x}. \tag{A.7}$$

Problem (A.6) can be solved explicitly, which yields

$$E_1^i(x) = (1-\varphi)\Big[\frac{x}{\delta} - \frac{C_i}{r^1} - \Big(\frac{b_i^1}{\delta} - \frac{C_i}{r^1}\Big)\Big(\frac{x}{b_i^1}\Big)^{\beta_1^i}\Big], \tag{A.8}$$

where β_1^i is the negative solution to $\frac{1}{2}\sigma_i^2\beta_1^i(\beta_1^i - 1) + (\mu_i - \sigma_i^2 + \sigma_i(\sigma_i - \rho\sigma_{-i})I_B)\beta_1^i - r^1 = 0$ and the smooth pasting condition determines b_i^1 to be

$$b_i^1 = \frac{\delta\beta_1^i C_i}{r^1(\beta_1^i - 1)}. \tag{A.9}$$

Similarly, we have $\lim_{s\to 1} D^i(x,s) =: D_1^i(x)$ and (A.5) reduces to

$$\begin{cases} \mathbb{L}^1_{X^i} D_1^i(x) - r^1 D_1^i(x) + C_i = 0, & x > b_i^1, \\ D_1^i(x) = (1-\epsilon)U^i(x,1), & x \le b_i^1. \end{cases} \tag{A.10}$$

It is also known from Cochrane et al. (2008), and is easy to show from (A.1), that $\lim_{s\to 1} V^i(s) = 1/\delta$, which yields

$$\lim_{s\to 1} U^i(x,s) = (1-\varphi)x \lim_{s\to 1} V^i(s) = (1-\varphi)\frac{x}{\delta}. \tag{A.11}$$

Therefore, solving problem (A.10), we obtain

$$D_i^1(x) = \frac{C_i}{r^1} + \Big[(1-\epsilon)(1-\varphi)\frac{b_i^1}{\delta} - \frac{C_i}{r^1}\Big]\Big(\frac{x}{b_i^1}\Big)^{\beta_1^i}. \tag{A.12}$$

A.2 The limit as $s \to 0$

The limit as $s \to 0$ corresponds to the solution to the problem when tree B dominates the economy and tree A is atomistic. In this limit $E^i(x,s) \to E_0^i(x)$ and the problem in (A.2) reduces to

$$\begin{cases} \mathbb{L}_{X^i}^0 E_0^i(x) - r^0 E_0^i(x) + (1-\varphi)(x - C_i) = 0, & x > b_i^0, \\ E_0^i(x) = 0, & x \le b_i^0, \\ \frac{dE_0^i}{dx}(x) = 0, & x = b_i^0, \end{cases} \tag{A.13}$$

where $r^0 = r(0) = \delta + \mu_B - \sigma_B^2$ and

$$\mathbb{L}_{X^i}^0 = \frac{1}{2}\sigma_i^2 x^2 \frac{\partial^2}{\partial x^2} + (\mu_i - \sigma_i^2 + \sigma_i(\sigma_i - \rho\sigma_{-i})1_A)x\frac{\partial}{\partial x}. \tag{A.14}$$

Under the assumption that $\nu + \psi > \eta^2$, problem (A.13) can be solved explicitly, yielding

$$E_0^i(x) = (1-\varphi)\Big[\frac{x}{\delta + \nu - \frac{1}{2}\eta^2} - \frac{C_i}{r^0} - \Big(\frac{b_i^0}{\delta + \nu - \frac{1}{2}\eta^2} - \frac{C_i}{r^0}\Big)\Big(\frac{x}{b_i^0}\Big)^{\beta_0^i}\Big], \tag{A.15}$$

where β_0^i is the negative solution to $\frac{1}{2}\sigma_i^2\beta_0^i(\beta_0^i - 1) + (\mu_i - \sigma_i^2 + \sigma_i(\sigma_i - \rho\sigma_{-i})1_A)\beta_0^i - r^0 = 0$.[25] Finally, the smooth pasting condition determines b_i^0 to be

$$b_i^0 = \frac{\beta_0^i C_i}{r^0(\beta_0^i - 1)}(\delta + \nu - \tfrac{1}{2}\eta^2). \tag{A.16}$$

Similarly, we have $\lim_{s\to 0} D^i(x,s) =: D_0^i(x)$ and (A.5) reduces to

$$\begin{cases} \mathbb{L}_{X^i}^0 D_0^i(x) - r^0 D_0^i(x) + C_i = 0, & x > b_i^0, \\ D_0^i(x) = (1-\epsilon)U^i(x,0), & x \le b_i^0. \end{cases} \tag{A.17}$$

It is also known from Cochrane et al. (2008), and is easy to show from (A.1), that $\lim_{s\to 0} V^i(s) =$

[25] If $\nu + \psi \le \eta^2$ then $E_0^i(x) \equiv \infty$, consistent with the infinite value of the unlevered tree in this parameter regime (see Cochrane et al., 2008).

$1/(\delta+\nu-\frac{1}{2}\eta^2)$ if $\nu+\psi\leq\eta^2$ (and ∞ otherwise), which under this condition yields

$$\lim_{s\to 0} U^i(x,s) = (1-\varphi)x \lim_{s\to 0} V^i(s) = \frac{(1-\varphi)x}{\delta+\nu-\frac{1}{2}\eta^2}. \tag{A.18}$$

Therefore, solving problem (A.10), we have

$$D_i^0(x) = \frac{C_i}{r^0} + \Big[\frac{(1-\epsilon)(1-\varphi)b_i^0}{\delta+\nu-\frac{1}{2}\eta^2} - \frac{C_i}{r^0}\Big]\Big(\frac{x}{b_i^0}\Big)^{\beta_0^i}. \tag{A.19}$$

B Proof of Proposition 1

This appendix outlines the computation of the correlation between the distances-to-default of the two borrowers, providing a proof to expression (12).

Proof. Working in the (X_t^A, X_t^B)-space rather the (X_t^A, s_t)-space, the boundary b_i becomes only a function of the other tree's output process X_t^{-i}. The distance-to-default of borrower i is then given by:

$$DD_t^i = \frac{1}{\sigma_i}\ln\Big(\frac{X_t^i}{b_i(X_t^{-i})}\Big), \quad \text{for } i=A,B, \tag{A.20}$$

where $b_i(X_t^{-i})$ denotes the default boundary of borrower i.

Applying Itô's formula to (A.20) yields

$$\begin{aligned} dDD_t^i &= \mu_{DD^i}(X_t^i, X_t^{-i})dt + dB_t^i - \frac{\sigma_{-i}}{\sigma_i}\frac{X_t^{-i}b_i'(X_t^{-i})}{b(X_t^{-i})}dB_t^{-i} \\ &= \mu_{DD^i}(X_t^i, X_t^{-i})dt + dB_t^i - \alpha_i f_i(X_t^{-i})dB_t^{-i}, \end{aligned} \tag{A.21}$$

where we have defined $\alpha_i = \sigma_{-i}/\sigma_i$ and $f_i(x) = xb_i'(x)/b_i(x)$, which denotes the *elasticity* of borrower i's default boundary to x, such that $f_i(X_t^{-i})$ is the elasticity of borrower i's default boundary to the output of the other borrower $(-i)$.

Defining $\rho_{DD}(X_t^A, X_t^B) = \mathrm{Corr}\big(dDD_t^A, dDD_t^B\big)$ and using $dB_t^i dB_t^{-i} = \rho dt$, it can be seen from (A.21) that

$$\rho_{DD}(X_t^A, X_t^B) = \frac{\rho[(1+f_A(X_t^B)f_B(X_t^A)] - \alpha_A f_A(X_t^B) - \alpha_B f_B(X_t^A)}{\sqrt{[1-2\rho\alpha_A f_A(X_t^B)+\alpha_A^2 f_A^2(X_t^B)][1-2\rho\alpha_B f_B(X_t^A)+\alpha_B^2 f_B^2(X_t^A)]}}. \tag{A.22}$$

While (A.22) is expressed in terms of (X_t^A, X_t^B), it can easily be converted to an expression in (X_t^A, s_t) by recalling that $s_t = X_t^A/(X_t^A + X_t^B)$, such that

$$b_A(X_t^B) = b_A(s_t) \;\&\; b'_A(X_t^B) = -\frac{s_t^2}{X_t^A} b'_A(s_t),$$
$$b_B(X_t^A) = b_B(s_t) \;\&\; b'_B(X_t^A) = \frac{s_t(1-s_t)}{X_t^A} b'_B(s_t).$$

Therefore, we have

$$f_A(X_t^B) = -s_t(1-s_t)\frac{b'_A(s_t)}{b_A(s_t)} \quad \text{and} \quad f_B(X_t^A) = s_t(1-s_t)\frac{b'_B(s_t)}{b_B(s_t)}. \tag{A.23}$$

Finally, defining $f_i(s) := s(1-s)b'_i(s)/b_i(s)$ and observing that $f_A(X_t^B) = -f_A(s_t)$ and $f_B(X_t^A) = f_B(s_t)$, we arrive at expression (12), completing the proof. □

C Additional results

This Appendix provides a robustness analysis and presents additional results not contained in the core of the paper. We first show that the results regarding the co-movement in default risk remain similar when we consider a bargaining game in default between shareholders and debtholders. We then explore how the degree of default risk co-movement varies with a borrower's characteristics.

C.1 Alternative specifications for recovery in default

We here verify that our key predictions are robust to changes in who gets what in default. Liquidation costs are a primary ingredient for corporate financing choices, but typically do not alter the default decision of a borrower (see Leland, 1994).[26] Therefore, for a given capital structure, the role of a costly liquidation might seem a second order concern. Yet, as Fan and Sundaresan (2000) show, when liquidation costs alter the outcome of bargaining in distress, then the ex post endogenous default decision does change. In addition, liquidation costs matter for the level of credit spreads insofar as they alter the payout to bondholders at default.

[26] The typical intuition is that, while the borrower bears liquidation costs ex ante via higher yields, the ex post impact is on the lenders who recover less in distress.

To account for these effects, we consider liquidation costs that are split between shareholders and bondholders. Specifically, bondholders now recover a fraction $1 - \epsilon/2$, while shareholders recover the fraction $\epsilon/2$ in default. This sharing rule can be viewed as the outcome of a Nash bargaining game between shareholders and bondholders, with equal bargaining power. Panel B of Table 2 shows that, accounting for costly liquidation in default, as in Fan and Sundaresan (2000), does not qualitatively change our findings regarding the transmission of default risk across borrowers.

C.2 The role of firm characteristics

It is reasonable to expect that borrower A's characteristics play a crucial role in determining its sensitivity to changes in borrower B's fundamentals, thereby influencing the extent of default risk co-movement. We explore whether this is the case.

Table A.1 demonstrates that the level of default risk correlation between the two borrowers slightly increases as borrower A features higher expected output growth (μ_A) and volatility (σ_A). This indicates that both dimensions contribute to amplifying borrower A's default risk exposure to shocks experienced by borrower B. However, it is important to note that the quantitative impact is relatively small.

Therefore, we can conclude that the degree of default risk co-movement is not critically dependent on the specific characteristics of a borrower. This finding emphasizes the robustness of our predictions.

TABLE A.1 ABOUT HERE

D Establishing the coupon independence of ρ_{DD}

This Appendix provides details on the coupon independence of the correlation between the changes in distances-to-default, $\rho_{DD}(s_t)$, defined in (12). Note that the expression (12) is valid for both our baseline model and our extension with rollover debt, developed in Section 3.1.

We see that the correlation is driven exclusively by the functions $f_i(s_t)$, which represent the sensitivity of the borrowers' default boundary to the output share s_t. This is key because a boundary $b_i(s)$ that scales linearly with the coupon C_i will result in a coupon-independent correlation, as we show

below. Consider the case that $b_i(s;C_i) = C_i b_i(s;1)$, we then obtain

$$f_i(s;C_i) = s(1-s)\frac{b_i'(s;C_i)}{b_i(s;C_i)} = s(1-s)\frac{C_i b_i'(s;1)}{C_i b_i(s;1)} = s(1-s)\frac{b_i'(s;1)}{b_i(s;1)} = f_i(s;1),$$

which proves that the sensitivities $f_i(s_t)$ are independent of the chosen coupon level C_i when the scaling property applies, and so is the correlation ρ_{DD}.

All that remains is to establish that the optimal default boundary scales linearly with the coupon level for both our baseline and extended model.

For the baseline model, this can be established directly from (8), which defines equity value. Specifically,

$$\begin{aligned} E^i(X_t^i, s_t; C_i) &= \sup_{\tau_i \geq t} \mathbb{E}_t\Big[\int_t^{\tau_i} \frac{M_u}{M_t}(1-\varphi)(X_u^i - C_i)du\Big] \\ &= C_i \sup_{\tau_i \geq t} \mathbb{E}_t\Big[\int_t^{\tau_i} \frac{M_u}{M_t}(1-\varphi)\big(\tfrac{X_u^i}{C_i} - 1\big)du\Big] \\ &= C_i E^i\big(\tfrac{X_t^i}{C_i}, s_t; 1\big), \end{aligned} \tag{A.24}$$

since the multiplicative nature of geometric Brownian motion means that the ratio X_u^i/C_i for $u \geq t$ is equivalent to a Brownian motion with the same dynamics but started at X_t^i/C_i, rather than X_t^i, at time t.

Since the equity value satisfies the scaling in (A.24) we see that the optimal default boundary for an arbitrary coupon C_i can be determined from the optimal stopping boundary for a unit coupon but whose output process starts at X_t^i/C_i. Hence $b_i(s_t;C_i) = C_i b_i(s_t;1)$, establishing the desired scaling in our baseline model.

Establishing the scaling property for the extended rollover debt model is a little more involved since the borrower's default decision depends directly on the valuation of debt. However, we can establish that the same scaling occurs in the debt valuation, defined in (10), with the following arguments. First, we observe from (9) that

$$U^i(X_t^i, s_t) = (1-\varphi)X_t^i V^i(s_t) = C_i(1-\varphi)\tfrac{X_t^i}{C_i}V^i(s_t) = C_i U^i(\tfrac{X_t^i}{C_i}, s_t)$$

and hence the rollover debt value can be written as

$$\begin{aligned} D^i(X_t^i, s_t; C_i) &= \mathbb{E}_t\Big[(C_i + m_i P_i)\int_t^{\tau_i} e^{-m_i(u-t)}\frac{M_u}{M_t}du + e^{-m_i(\tau_i - t)}\frac{M_{\tau_i}}{M_t}(1-\epsilon)C_i U^i(\tfrac{X^i_{\tau_i}}{C_i}, s_{\tau_i})\Big] \\ &= C_i\mathbb{E}_t\Big[(1 + m_i\hat{P}_i)\int_t^{\tau_i} e^{-m_i(u-t)}\frac{M_u}{M_t}du + e^{-m_i(\tau_i - t)}\frac{M_{\tau_i}}{M_t}(1-\epsilon)U^i(\tfrac{X^i_{\tau_i}}{C_i}, s_{\tau_i})\Big] \\ &= C_i D^i(\tfrac{X_t^i}{C_i}, s_t; 1), \end{aligned} \tag{A.25}$$

where we have assumed that the total face value P_i is proportional to the coupon level C_i, and thus $\hat{P}_i = P_i/C_i$ is a coupon-independent constant. In our baseline parameterization in Section 3.1, we set $P_i = C_i/r(0.5)$, hence $\hat{P}_i = 1/r(0.5)$.

Finally, given the scaling in (A.25), we can establish the scaling in the rollover equity value in (20) as follows:

$$\begin{aligned} E^i(X_t^i, s_t; C_i) &= \sup_{\tau_i \geq t}\mathbb{E}_t\Big[\int_t^{\tau_i}\frac{M_u}{M_t}\big[(1-\varphi)(X_u^i - C_i) + m_i(D(X_u^i, s_u; C_i) - P_i)\big]du\Big] \\ &= C_i\sup_{\tau_i \geq t}\mathbb{E}_t\Big[\int_t^{\tau_i}\frac{M_u}{M_t}\big[(1-\varphi)(\tfrac{X_u^i}{C_i} - 1) + m_i(D\big(\tfrac{X_u^i}{C_i}, s_u; 1\big) - \hat{P}_i)\big]du\Big] \\ &= C_i E^i\big(\tfrac{X_t^i}{C_i}, s_t; 1\big). \end{aligned}$$

Hence, the optimal default boundary scales linearly with the coupon choice, establishing the coupon independence of ρ_{DD} in both the baseline and the rollover debt cases.

E Equity return volatility and equity risk premium

This Appendix derives the equity return volatility and equity risk premium of the levered trees. The expressions for the debt return volatility and debt risk premium are obtained by simply replacing E^i for D^i in (A.30) and (A.33), respectively.

The equity value of levered tree i, denoted by $E_t^i = E^i(X_t^i, s_t)$, is a function of the following two state variables:

$$\frac{dX_t^i}{X_t^i} = \mu_i dt + \sigma_i dB_t^i \tag{A.26}$$

$$ds_t = s_t(1-s_t)\big[\alpha(s_t)dt + \sigma_A dB_t^A - \sigma_B dB_t^B\big], \tag{A.27}$$

where

$$\alpha(s_t) = \mu_A - \mu_B - s_t\sigma_A^2 + (1-s_t)\sigma_B^2 + 2(s_t - 1/2)\rho\sigma_A\sigma_B. \tag{A.28}$$

Using Itô's formula, the equity value of levered tree i has the following dynamics:

$$\begin{aligned} dE_t^i = \Bigg\{ & \frac{\partial E_t^i}{\partial X_t^i} X_t^i \mu_i + \frac{\partial E_t^i}{\partial s_t} s_t(1-s_t)\alpha(s_t) + \frac{1}{2}\frac{\partial^2 E_t^i}{\partial {X_t^i}^2} {X_t^i}^2 \sigma_i^2 + \frac{1}{2}\frac{\partial E_t^i}{\partial s_t^2} s_t^2 (1-s_t)^2 \eta^2 \\ & + \frac{\partial^2 E_t^i}{\partial X_t^i \partial s_t} X_t^i s_t(1-s_t)\sigma_i(\sigma_i - \rho\sigma_{-i})(I_A - I_B) \Bigg\} dt \\ & + \left[\frac{\partial E_t^i}{\partial X_t^i} X_t^i \sigma_i + \frac{\partial E_t^i}{\partial s_t} s_t(1-s_t)\sigma_i(I_A - I_B) \right] dB_t^i - \frac{\partial E_t^i}{\partial s_t} s_t(1-s_t)\sigma_{-i}(I_A - I_B) dB_t^{-i} \end{aligned} \tag{A.29}$$

where $\eta^2 = \sigma_i^2 + \sigma_{-i}^2 - 2\rho\sigma_i\sigma_{-i}$ and I_j denotes the indicator function which is equal to 1 when $i = j$, and zero otherwise.

The conditional equity variance is then given by

$$\begin{aligned} \text{var}_{E^i,t} = & \left[\frac{\partial E_t^i}{\partial X_t^i} X_t^i \sigma_i + \frac{\partial E_t^i}{\partial s_t} s_t(1-s_t)\sigma_i(I_A - I_B) \right]^2 + \left[\frac{\partial E_t^i}{\partial s_t} s_t(1-s_t)\sigma_{-i}(I_A - I_B) \right]^2 \\ & - 2\rho \left[\frac{\partial E_t^i}{\partial X_t^i} X_t^i \sigma_i + \frac{\partial E_t^i}{\partial s_t} s_t(1-s_t)\sigma_i(I_A - I_B) \right] \left[\frac{\partial E_t^i}{\partial s_t} s_t(1-s_t)\sigma_{-i}(I_A - I_B) \right] \end{aligned} \tag{A.30}$$

such that the equity return volatility equals $\sigma_{E^i,t} = \sqrt{\text{var}_{E^i,t}/(E_t^i)^2}$. As there is no closed-form solution for the equity value, we need to evaluate the two first-order derivatives $\frac{\partial E_t^i}{\partial X_t^i}$ and $\frac{\partial E_t^i}{\partial s_t}$ numerically.

To compute the equity risk premium, we note that

$$ERP_t^i = \underbrace{\frac{1}{dt}\mathbb{E}_t\left[\frac{dE_t^i + (1-\varphi)(X_t^i - C_i)dt}{E_t^i}\right]}_{\text{Expected (total) return on equity, } R_t} - \underbrace{r(s_t)}_{\text{Risk-free rate}} \tag{A.31}$$

where, from (A.29), we have

$$\begin{aligned} R_t = \frac{1}{E_t^i}\Big[& \frac{\partial E_t^i}{\partial X_t^i} X_t^i \mu_i + \frac{\partial E_t^i}{\partial s_t} s_t(1-s_t)\alpha(s_t) + \frac{1}{2}\frac{\partial^2 E_t^i}{\partial {X_t^i}^2} {X_t^i}^2 \sigma_i^2 + \frac{1}{2}\frac{\partial E_t^i}{\partial s_t^2} s_t^2(1-s_t)^2\eta^2 \\ & + \frac{\partial^2 E_t^i}{\partial X_t^i \partial s_t} X_t^i s_t(1-s_t)\sigma_i(\sigma_i - \rho\sigma_{-i})(I_A - I_B) + (1-\varphi)(X_t^i - C_i) \Big]. \end{aligned} \tag{A.32}$$

However, noting that $E^i(X_t^i, s_t)$ must satisfy the differential equation in (A.2), our expression for ERP_t^i in (A.31)-(A.32) simplifies to

$$\begin{aligned} ERP_t^i = & \frac{1}{E_t^i}\frac{\partial E_t^i}{\partial X_t^i} X_t^i \big[\sigma_i^2 - \sigma_i(\sigma_i - \rho\sigma_{-i})(I_A + (I_B - I_A)s_t)\big] \\ & + \frac{1}{E_t^i}\frac{\partial E_t^i}{\partial s_t} s_t(1-s_t)\big[\eta^2 s_t - \sigma_B(\sigma_B - \rho\sigma_A)\big]. \end{aligned} \tag{A.33}$$

F The default probability

This Appendix describes the computation of a borrower's default probability, when its default boundary, $b^i(s)$, is determined from the solution to problem (8). We show that the probabilities under both the physical risk-neutral measures can be computed via the numerical solution of a time-dependent partial differential equation (PDE) with two state variables (i.e., X_t^i and s_t).

Under the physical measure, the dynamics of X_t^i and s_t are given by (1) and (3), respectively. Setting $X_t^i = x$ and $s_t = s$, the physical default probability $\mathbb{P}_{x,s}(\tau_i < T)$, for a fixed horizon T, is given by the solution to the following boundary-value problem (for $i = A, B$):

$$\begin{cases} \frac{\partial}{\partial t}P^i(t,x,s) + \mathbb{L}^P_{(X^i,s)}P^i(t,x,s) = 0, & \text{for } x > b^i(s) \text{ and } t \in [0,T), \\ P^i(t,x,s) = 1, & \text{for } x \leq b^i(s) \text{ and } t \in [0,T), \\ P^i(t,x,s) = 1_{\{x<b^i(s)\}}, & \text{at } t = T, \text{ for all } x, \end{cases} \tag{A.34}$$

where $\mathbb{L}^P_{(X^i,s)}$ is the infinitesimal generator of the two-dimensional diffusion (X_t^i, s_t) under the physical measure, given by

$$\begin{aligned} \mathbb{L}^P_{(X^i,s)} = & \frac{1}{2}\sigma_i^2 x^2 \frac{\partial^2}{\partial x^2} + \frac{1}{2}\eta^2 s^2(1-s)^2\frac{\partial^2}{\partial s^2} + \sigma_i(\sigma_i - \rho\sigma_{-i})(I_A - I_B)xs(1-s)\frac{\partial^2}{\partial x \partial s} \\ & + \mu_i x\frac{\partial}{\partial x} + \alpha(s)s(1-s)\frac{\partial}{\partial s}, \end{aligned} \tag{A.35}$$

where $\alpha(s)$ is as given in (A.4). Note that line two in (A.34) ensures that the default probability is equal to one at all points when borrower i defaults. Moreover, line three ensures that the default probability at maturity T is either zero or one, depending on whether the borrower's output is above or below the default boundary.

The solution to problem (A.34) is approximated numerically via standard finite-difference methods. Specifically, we discretize the PDE using a Crank-Nicolson differencing scheme to account for the time variation in the probability. We then use backward time-stepping, from $t = T$ where the solution is known; see line 3 in (A.34). At each time step, the resulting linear system of algebraic equations is solved via an iterative Successive Over Relaxation (SOR) algorithm (see Smith, 1985). Using a Crank-Nicolson discretization allows the use of larger timesteps due to the unconditional stability imposed by the scheme, and the SOR method allows for faster convergence than the simpler Gauss–Seidel method. A more detailed description of the discretization and implementation of the algorithm can be made available from the authors upon request.

The risk-neutral probability can be determined via an equivalent boundary-value problem to (A.34), but whose infinitesimal generator is given by $\mathbb{L}_{(X^i,s)}$, defined in (A.3). Specifically, the risk-neutral default probability, Q^i, is given by:

$$\begin{cases} \frac{\partial}{\partial t}Q^i(t,x,s) + \mathbb{L}_{(X^i,s)}Q^i(t,x,s) = 0, & \text{for } x > b^i(s) \text{ and } t \in [0,T), \\ Q^i(t,x,s) = 1, & \text{for } x \leq b^i(s) \text{ and } t \in [0,T), \\ Q^i(t,x,s) = 1_{\{x<b^i(s)\}}, & \text{at } t = T, \text{ for all } x. \end{cases} \tag{A.36}$$

The solution to (A.36) is approximated numerically using the same method as for the physical probability problem given in (A.34).

G Simulation analysis

This Appendix describes the simulation procedure discussed in Section 2.8. We simulate 20,000 two-tree economies at the daily frequency over a 10-year period. Specifically, for each economy we simulate each tree's output process, given by (1), for 2,520 daily periods (assuming 252 trading days per year). We further assume that the Brownian shocks are independent across trees to highlight the *excess* default risk correlation induced by the mechanism proposed in this paper.

G.1 Baseline model

Given each tree's output level at time t, the output share s_t is computed. Should a tree's output level drop below the default boundary $b^i(s_t)$, then a default occurs and that tree's output level is set to zero for all remaining periods; hence the output share process jumps to either zero or one, depending on which tree defaults. In the event of a second default in the 10-year period, the simulation ends for this particular economy.

Next, given each simulated path of the process (X_t^i, s_t), we obtain the associated sample paths of each tree's distance-to-default and other metrics presented in Table 3. This yields two time-series (one for each tree) for each of our metrics of interest. For each economy, we compute the empirical correlation of each metric between the two trees, using data up to the time of the first default (or all 10 years if no defaults occur in a given economy). We then average these correlations across economies and compute their 5th, 50th, and 95th percentiles.

To generate an initial cross-section of economies, each tree starts at $t = 0$ with an output level drawn randomly between 0.25 and 1.50, such that the initial distance-to-default varies across trees. Since both trees are drawn independently from the same distribution, there will also be variation in the initial output share level, with the expected output share across simulations equal to 0.5. This initial output distribution is calibrated such that the simulated default frequencies match those observed empirically. As reported in Panel A of Table 3, the average cumulative 1-, 5-, and 10-year default rates are 1.41%, 6.29%, and 11.79% across the simulated economies, while they are respectively 1.86%, 7.72%, and 11.37% based on the cumulative default rates for all-rated corporate bonds in the U.S. from Standard and Poor's (2021). The model parameters and the initial output distribution are therefore properly calibrated. Table 3 presents the full simulation results for the correlations between default risk measures in Panel B and asset pricing moments in Panel C.

In addition, we present the sampling distributions of our simulations based on default risk metrics and asset pricing moments in Figures A.1 and A.2, respectively. We can clearly see that the correlations across trees in our model are significantly different from zero.

FIGURES A.1 and A.2 ABOUT HERE

G.2 Counterfactual analysis

For comparison, we repeat the above simulation procedure for the counterfactual case of borrowers with constant default boundaries, so that a borrower's default policy is independent of the fate of the other borrower. One can view this as a scenario of two separate economies, each with one borrower, instead of one economy with two borrowers.

Specifically, we replace the endogenous default boundary $b(s_t)$ with a static boundary $b(s_0)$, corresponding to the default boundary applicable to the initial state of the economy s_0. Thus, each tree's default decision no longer depends on stochastic fluctuations in the output share, effectively cutting off the default risk linkage channel described in this paper. In such simulations, we should therefore expect that the correlation between trees for any metric is, on average, zero. Importantly however, the distribution of simulated correlations across samples with a static boundary gives a clean indication of the sampling error introduced by our simulation procedure in the absence of the default linkage channel. To help with comparisons between the static and stochastic boundary simulations, we also choose to use the same random numbers across both simulations. The results reported in Figures A.1 and A.2 are clearly shifted towards the left and centered around zero in this exercise. The results obtained in the base case are significantly different from those counterfactual results and, therefore, unlikely due to random occurrence.

H Security valuation with rollover debt

This Appendix derives the expressions for the value of finite-maturity debt and the corresponding equity, respectively given in (18) and (20). It also provides details on the numerical solution procedure.

H.1 Deriving the value of debt in equation (18)

First substitute (17) into (16) and perform the following manipulations:

$$\begin{aligned}
D^i(X_t^i, s_t) &= \int_0^\infty e^{-m_i T} p_i d^i(X_t^i, s_t; T) dT \\
&= \mathbb{E}_t\Big[p_i c_i \int_{T=0}^\infty \int_{u=t}^{t+T} \frac{M_u}{M_t} e^{-m_i T} I_{\{\tau_i > u\}} du dT + p_i \int_0^\infty \frac{M_{t+T}}{M_t} e^{-m_i T} I_{\{\tau_i > t+T\}} dT \\
&\qquad + (1-\epsilon)\frac{p_i}{P_i} \int_0^\infty \frac{M_{\tau_i}}{M_t} U^i(X_{\tau_i}^i, s_{\tau_i}) e^{-m_i T} I_{\{\tau_i \le t+T\}} dT\Big] \\
&= \mathbb{E}_t\Big[p_i c_i \int_{u=t}^\infty \frac{M_u}{M_t} \Big(\int_{T=u-t}^\infty e^{-m_i T} dT\Big) I_{\{\tau_i > u\}} du + p_i \int_0^{\tau_i - t} \frac{M_{t+T}}{M_t} e^{-m_i T} dT \\
&\qquad + (1-\epsilon)\frac{p_i}{P_i}\frac{M_{\tau_i}}{M_t} U^i(X_{\tau_i}^i, s_{\tau_i}) \int_0^\infty e^{-m_i T} I_{\{\tau_i \le t+T\}} dT\Big] \\
&= \mathbb{E}_t\Big[\frac{p_i c_i}{m_i} \int_t^{\tau_i} e^{-m_i(u-t)} \frac{M_u}{M_t} du + p_i \int_t^{\tau_i} \frac{M_u}{M_t} e^{-m_i(u-t)} du \\
&\qquad + (1-\epsilon)\frac{p_i}{m_i P_i}\frac{M_{\tau_i}}{M_t} U^i(X_{\tau_i}^i, s_{\tau_i}) e^{-m_i(\tau_i - t)}\Big] \\
&= \mathbb{E}_t\Big[(C_i + m_i P_i) \int_t^{\tau_i} e^{-m_i(u-t)} \frac{M_u}{M_t} du + e^{-m_i(\tau_i - t)} \frac{M_{\tau_i}}{M_t} (1-\epsilon) U^i(X_{\tau_i}^i, s_{\tau_i})\Big],
\end{aligned}$$

where we use $p_i c_i / m_i = c_i P_i = C_i$ and $p_i = m_i P_i$ to obtain the last equality.

H.2 Numerical procedure for the rollover model

We assume that the optimal default time in (20) is of the form $\tau_i = \inf\{u \ge t \,|\, X_u^i \le b_{i,m}(s_u)\}$. Setting $X_t^i = x$ and $s_t = s$ reveals that borrower i's optimal stopping problem must also satisfy the following free-boundary problem:

$$\begin{cases}
\mathbb{L}_{(X^i,s)} E^i(x,s) - r(s) E^i(x,s) + (1-\varphi)(x - C_i) + m_i(D^i(x,s) - P_i) = 0, & x > b_{i,m}(s), \\
E^i(x,s) = 0, & x \le b_{i,m}(s), \\
\frac{\partial E^i}{\partial x}(x,s) = 0 \text{ and } \frac{\partial E^i}{\partial s}(x,s) = 0, & x = b_{i,m}(s),
\end{cases} \tag{A.37}$$

where $r(s)$ is the risk-free rate defined in (7) and $\mathbb{L}_{(X^i,s)}$ is the infinitesimal generator of the two-dimensional diffusion (X_t^i, s_t) under the risk-neutral measure given in equation (A.3).

Similarly, the debtholders' problem in (18) must also satisfy the following fixed-boundary problem:

$$\begin{cases} \mathbb{L}_{(X^i,s)} D^i(x,s) - (r(s)+m_i) D^i(x,s) + C_i + m_i P_i = 0, & x > b_{i,m}(s), \\ D^i(x,s) = (1-\epsilon) U^i(x,s), & x \leq b_{i,m}(s). \end{cases} \tag{A.38}$$

Recall that, in the perpetual debt model outlined in Section 1, the borrower's default decision does not depend on the value of debt. In other words, the (perpetual) equity free-boundary problem can be solved first to determine the stopping boundary b_i and then the debt problem can be solved subsequently, given the computed b_i. In the presence of rollover risk, however, the debt and equity boundary value problems, given in (A.37) and (A.38), are coupled due to the value of debt entering into the borrower's cash flow. Hence, the two boundary value problems must be solved jointly.

To approximate the solution to (A.37) and (A.38) numerically, we discretize both problems using a second-order finite differencing scheme. The resulting system of *coupled* equations are then solved iteratively using an approximation for the default boundary from the PSOR algorithm *at each iteration* as the boundary for the debt equation, and the approximated debt value from the SOR algorithm *at each iteration* in the equity equation. This process is then repeated until convergence. More details about the discretization and implementation of the algorithm can be made available from the authors upon request.

In order to obtain accurate results for the numerical solution to (A.37) and (A.38), we need to correctly define the boundary conditions on both E^i and D^i for $s = 0$ and $s = 1$. The limiting optimal stopping problems are solvable in closed form, as we show below.

H.2.1 The limit as $s \to 1$

Setting $E_1^i(x) := \lim_{s\to 1} E^i(x,s)$ and $D_1^i(x) := \lim_{s\to 1} D^i(x,s)$, problems (A.37) and (A.38) reduce to the following as $s \to 1$:

$$\begin{cases} \mathbb{L}^1_{X^i} E_1^i(x) - r^1 E_1^i(x) + (1-\varphi)(x - C_i) + m_i(D_1^i(x) - P_i) = 0, & x > b^1_{i,m}, \\ E_1^i(x) = 0, & x \leq b^1_{i,m}, \\ \frac{dE_1^i}{dx}(x) = 0, & x = b^1_{i,m}, \end{cases} \tag{A.39}$$

and

$$\begin{cases} \mathbb{L}^1_{X^i} D^i_1(x) - (r^1 + m_i) D^i_1(x) + C_i + m_i P_i = 0, & x > b^1_{i,m}, \\ D^i_1(x) = (1-\epsilon) U^i(x,1), & x \le b^1_{i,m}, \end{cases} \tag{A.40}$$

where, as before, $r^1 = \delta + \mu_A - \sigma_A^2$ and $\mathbb{L}^1_{X^i}$ is defined in (A.7).

Given a putative boundary $b^1_{i,m}$, problem (A.40) can be solved explicitly yielding

$$D^i_1(x) = \frac{C_i + m_i P_i}{r^1 + m_i} + \Big[(1-\epsilon)(1-\varphi)\frac{b^1_{i,m}}{\delta} - \frac{C_i + m_i P_i}{r^1 + m_i}\Big]\Big(\frac{x}{b^1_{i,m}}\Big)^{\beta_1^{i,m}}, \tag{A.41}$$

where $\beta_1^{i,m}$ is the negative solution to $\frac{1}{2}\sigma_i^2\beta_1^{i,m}(\beta_1^{i,m}-1)+(\mu_i-\sigma_i^2+\sigma_i(\sigma_i-\rho\sigma_{-i})I_B)\beta_1^{i,m}-r^1-m_i=0$. Equation (A.41) can then be substituted into (A.39) which can then be solved explicitly, revealing

$$\begin{aligned} E^i_1(x) = (1-\varphi)\frac{x}{\delta} - \Big[\frac{\varphi C_i}{r^1} + \epsilon(1-\varphi)\frac{b^1_{i,m}}{\delta}\Big]\Big(\frac{x}{b^1_{i,m}}\Big)^{\beta_1^i} \\ + \frac{\varphi C_i}{r^1} - \frac{C_i + m_i P_i}{r^1 + m_i} - \Big[(1-\epsilon)(1-\varphi)\frac{b^1_{i,m}}{\delta} - \frac{C_i + m_i P_i}{r^1 + m_i}\Big]\Big(\frac{x}{b^1_{i,m}}\Big)^{\beta_1^{i,m}}, \end{aligned} \tag{A.42}$$

where β_1^i is the negative solution to $\frac{1}{2}\sigma_i^2\beta_1^i(\beta_1^i-1)+(\mu_i-\sigma_i^2+\sigma_i(\sigma_i-\rho\sigma_{-i})I_B)\beta_1^i-r^1=0$. Finally, the smooth pasting condition applied to (A.42) yields

$$b^1_{i,m} = \frac{\delta}{(1-\varphi)\big(1-\epsilon\beta_1^i-(1-\epsilon)\beta_1^{i,m}\big)}\Big[\frac{\varphi C_i}{r^1}\beta_1^i - \frac{C_i + m_i P_i}{r^1 + m_i}\beta_1^{i,m}\Big]. \tag{A.43}$$

Pleasingly, as $m_i \to 0$, corresponding to static perpetual debt, we see that $\beta_1^{i,m} \to \beta_1^i$ and $b^1_{i,m} \to b^1_i$, given in (A.9).

H.2.2 The limit as $s \to 0$

Setting $E^i_0(x) := \lim_{s\to 0} E^i(x,s)$ and $D^i_0(x) := \lim_{s\to 0} D^i(x,s)$, problems (A.37) and (A.38) reduce to the following as $s \to 0$:

$$\begin{cases} \mathbb{L}^0_{X^i} E^i_0(x) - r^0 E^i_0(x) + (1-\varphi)(x - C_i) + m_i(D^i_0(x) - P_i) = 0, & x > b^0_{i,m}, \\ E^i_0(x) = 0, & x \le b^0_{i,m}, \\ \frac{dE^i_0}{dx}(x) = 0, & x = b^0_{i,m}, \end{cases} \tag{A.44}$$

and

$$\begin{cases} \mathbb{L}^0_{X^i} D^i_0(x) - (r^0 + m_i) D^i_0(x) + C_i + m_i P_i = 0, & x > b^0_{i,m}, \\ D^i_0(x) = (1-\epsilon) U^i(x, 0), & x \le b^0_{i,m}, \end{cases} \tag{A.45}$$

where, as before, $r^0 = \delta + \mu_B - \sigma_B^2$ and $\mathbb{L}^0_{X^i}$ is defined in (A.14).

Given a putative boundary $b^0_{i,m}$, problem (A.45) can be solved explicitly yielding

$$D^i_0(x) = \frac{C_i + m_i P_i}{r^0 + m_i} + \Big[(1-\epsilon)(1-\varphi)\frac{b^0_{i,m}}{\delta} - \frac{C_i + m_i P_i}{r^0 + m_i}\Big]\Big(\frac{x}{b^0_{i,m}}\Big)^{\beta_0^{i,m}}, \tag{A.46}$$

where $\beta_0^{i,m}$ is the negative solution to $\frac{1}{2}\sigma_i^2\beta_0^{i,m}(\beta_0^{i,m}-1)+(\mu_i-\sigma_i^2+\sigma_i(\sigma_i-\rho\sigma_{-i})1_A)\beta_0^{i,m}-r^0-m_i=0$. Substituting (A.46) into (A.44), which can then be solved explicitly, we obtain,under the assumption that $\nu + \psi > \eta^2$, that:

$$\begin{aligned} E^i_0(x) = {} & \frac{(1-\varphi)x}{\delta + \nu - \frac{1}{2}\eta^2} - \Big[\frac{\varphi C_i}{r^0} + \frac{\epsilon(1-\varphi)b^0_{i,m}}{\delta + \nu - \frac{1}{2}\eta^2}\Big]\Big(\frac{x}{b^0_{i,m}}\Big)^{\beta_0^i} + \frac{\varphi C_i}{r^0} \\ & - \frac{C_i + m_i P_i}{r^0 + m_i} - \Big[\frac{(1-\epsilon)(1-\varphi)b^0_{i,m}}{\delta + \nu - \frac{1}{2}\eta^2} - \frac{C_i + m_i P_i}{r^0 + m_i}\Big]\Big(\frac{x}{b^0_{i,m}}\Big)^{\beta_0^{i,m}}, \end{aligned} \tag{A.47}$$

where β_0^i is the negative solution to $\frac{1}{2}\sigma_i^2\beta_0^i(\beta_0^i - 1) + (\mu_i - \sigma_i^2 + \sigma_i(\sigma_i - \rho\sigma_{-i})1_A)\beta_0^i - r^0 = 0$.[27] Finally, the smooth pasting condition applied to (A.47) yields

$$b^0_{i,m} = \frac{\delta + \nu - \frac{1}{2}\eta^2}{(1-\varphi)\big(1 - \epsilon\beta_0^i - (1-\epsilon)\beta_0^{i,m}\big)}\Big[\frac{\varphi C_i}{r^0}\beta_0^i - \frac{C_i + m_i P_i}{r^0 + m_i}\beta_0^{i,m}\Big]. \tag{A.48}$$

Again, as $m_i \to 0$, we can see that $\beta_0^{i,m} \to \beta_0^i$ and $b^0_{i,m} \to b^0_i$, given in (A.16).

[27] Recall that the equity value will be infinite if $\nu + \psi \le \eta^2$.

Table A.1. Default risk correlation by firm characteristics

This table reports the correlation between distances-to-default of trees A and B (given by ρ_{DD}) for varying firm characteristics. Each column considers a different level of expected output growth (μ_A), while each row considers a different level of output growth volatility (σ_A). The output shocks are independent across trees ($\rho = 0$). Section 2.1 discusses the model calibration.

	Expected output growth (μ_A)		
	1.5%	2.0%	2.5%
Output volatility (σ_A)			
15%	7.14%	8.18%	9.17%
20%	8.76%	9.51%	10.42%
25%	10.04%	10.86%	11.58%

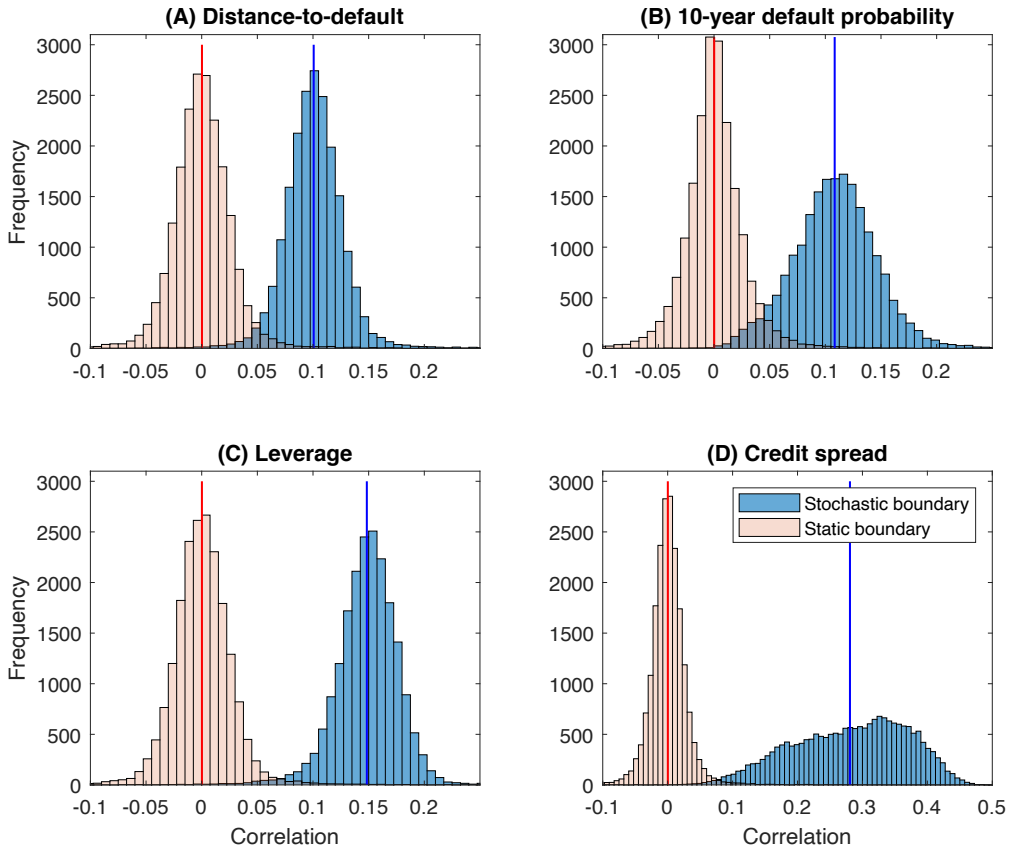

Figure A.1. The Distribution of default risk correlation

This figure plots the distribution of the correlation in default risk across trees based on model simulations. We simulate 20,000 two-tree economies at the daily frequency over a 10-year period using the parameters of the baseline calibration in Table 1. Each panel reports the distribution of the unconditional default-risk correlation based on all simulations. The full model with optimal stochastic default boundary, at the core of the default-risk co-movement across trees, is compared to the case of a static default boundary. Panel A has the distance-to-default, Panel B has the default probability computed at the 10-year horizon, Panel C has the leverage ratio, and Panel D has the credit spread. The vertical lines illustrate the averaged correlation levels. Section 2.1 discusses the model calibration, while Appendix G provides details on the simulation procedure.

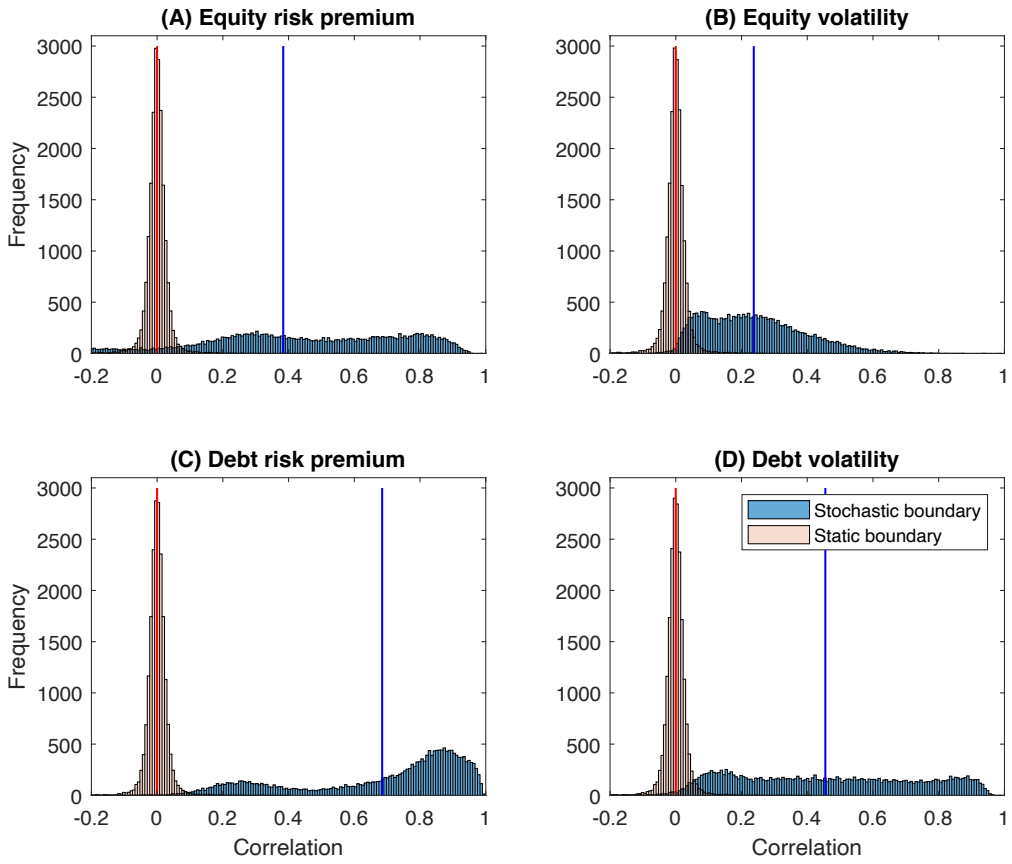

Figure A.2. Distribution of the correlations in asset pricing moments

This figure plots the distribution of the correlation in asset pricing moments across trees based on model simulations. We simulate 20,000 two-tree economies at the daily frequency over a 10-year period using the parameters of the baseline calibration in Table 1. Each panel reports the distribution of the unconditional asset pricing moment based on all simulations. The full model with optimal stochastic default boundary, at the core of the default risk co-movement across trees, is compared to the case of a static default boundary. Panel A has the equity risk premium, Panel B has the equity volatility, Panel C has the debt risk premium, and Panel D has the debt volatility. The vertical lines illustrate the averaged correlation levels. Section 2.1 discusses the model calibration, while Appendix G provides details on the simulation procedure.

fbe.unimelb.edu.au/finance